Univerzita Karlova

1. lékařská fakulta

Studijní program: Biomedicína
Studijní obor: Zobrazovací metody v lékařství

UNIVERZITA KARLOVA
1. lékařská fakulta

Ing. Daniel Tureček

Algoritmy pro multi-modální radiografii s novými zobrazovacími detektory

Algorithms for multimodal radiography with novel imaging detectors

Disertační práce

Školitel: RNDr. Luděk Šefc, CSc.

Konzultant: Ing. Jan Jakůbek, Ph.D.

Praha 2019

Prohlášení

Prohlašuji, že jsem závěrečnou práci zpracoval samostatně a že jsem řádně uvedl a citoval všechny použité prameny a literaturu. Současně prohlašuji, že práce nebyla využita k získání jiného nebo stejného titulu.

Souhlasím s trvalým uložením elektronické verze mé práce v databázi systému meziuniverzitního projektu Theses.cz za účelem soustavné kontroly podobnosti kvalifikačních prací.

V Praze, 30.09.2019

Daniel Tureček

Identifikační záznam

Tureček, Daniel. *Algoritmy pro multi-modální radiografii s novými zobrazovacími detektory [Algorithms for multimodal radiography with novel imaging detectors]*. Praha 2019, 85 s, 5 příl. Disertační práce. Univerzita Karlova v Praze, 1. lékařská fakulta, Školitel: RNDr. Luděk Šefc, CSc.

Acknowledgement

First of all, I would like to thank my supervisor-specialist Ing. Jan Jakůbek, Ph.D. for his guiding, advices and help with this work. I appreciate his deep knowledge of the subject, provided encouragement and a lots of great ideas. I would like to also thank my supervisor RNDr. Luděk Šefc CSc., for his supervision and advices. Lastly, I would like to thank my girlfriend and family for their support while I was working on this thesis.

Abstract

Medical imaging is a technique that allows us to visualize non surgically the internal structure of the human body in order to diagnose or treat medical conditions. It permits also monitoring of physical processes or functions of different organs inside the body. The medical imaging encompasses wide range of techniques based on different physical principles, including techniques using ionizing radiation. The quality of the images depends significantly on the quality of the used imaging detectors. There are many types of the detectors, from old analog devices (e.g. films) to fully digital detectors such as flat panels, that are the most widely used today. The newer technology is being developed and the techniques such as photon counting explored. However, the state of the art technology is the single photon counting, where the experimental detectors such as Medipix are able to count and process each individual photon.

This works studies the properties, features and applications of the newest detector from the Medipix family Timepix3 in different imaging modalities. Firstly, a design of a new hardware readout interface for Timepix3 is presented together with data acquisition software and new analysis and calibration algorithms. Then, different applications of Timepix3 detector were explored: very fast full spectral radiography - demonstrates a very fast measurement of "color" X-ray radiography. Single Photon Emission Tomography (SPECT) - benefited from using Timepix3 detector with suppression of unwanted signal, high resolution and energy sensitivity. The Positron Emission Tomography (PET) applications exploited the timing properties of Timepix3 to find coincidence gammas from positron annihilation as well as energy properties that helped to suppress massively the unwanted signal (by two orders of magnitude). Finally, application of the Compton camera concept has been studied. A multilayer and a miniaturized single layer Compton cameras designs are presented. The main advantage of these cameras is the possibility to avoid collimator in SPECT imaging and increase vastly sensitivity of the method. We have also proved other advantages of these cameras: times better resolution compared to the conventional gamma cameras, small dimensions (USB flash stick size), and weight (only 15 g).

This work also demonstrates that the use of single photon counting detectors such as Timepix3 significantly improved the quality of images in medical imaging and could even open in the future new imaging modalities and applications that were not possible before.

Keywords: Medical Imaging, Medipix, Timepix3, SPECT, PET, Compton camera

Abstrakt

Zobrazování v medicíně je technika, která nám umožňuje bez operativních zásahů vizualizovat vnitřní struktury lidského těla, abychom mohli diagnostikovat nemoci. Umožňuje nám taky monitorování fyzikálních procesů a funkcí různých orgánů v těle. Obor medicínského zobrazování obsahuje širokou škálu metod založených na různých fyzikálních principech. Součástí tohoto oboru jsou i metody používající ionizující záření. Kvalita naměřených snímků silně závisi na použitých zobrazovacích detektorech. Existuje celá řada různých typů detektorů, od čistě analogových (filmy) až po plně digitální detektory jako jsou flat panely, které jsou v dnešní době nejrozšířenější. Novější typy dektorů využívají technologie počítání fotonů a nejmodernější experimentální detektory jako například Medipix jsou schopné detekovat a analyzovat jednotlivé fotony.

Tato práce studuje vlastnoti, parametery a možné aplikační využití nejvnovejšího detektoru Timepix3 z rodiny detektorů Medipix v různých zobrazovacích modalitách. Nejprve byl vyvinut nový vyčítací hardware a akviziční software společně s novými kalibračními a korekčními metodami. Poté byly postupně prozkoumány různé módy Timepix3 detektoru: velmi rychlá spektrální radiografie, která demonstruje velmi rychlé měření "barevných" rentgenových obrázků; jednofotovná emisní výpočetní tomografie (SPECT), která demonstruje výhody Timepix3 detektoru jako: potlačení nežádoucího signálu, vysoké rozlišení a energetická citlivost. Pozitronová emissní tomografie (PET) aplikace pak využívá časového měření k nalezení koincidenčních gamma událostí z anihilace positronů. Energetické měření navíc pomáhá potlačit nežádoucí signál až o dva řády. V poslední části práce je pak studován koncept Comptonovy kamery a je prezentován design vícevrstvé a miniaturní jednovrstvé Comptnovy kamery. Vyhodou těchto kamer je až 6 krát lepsí rozlišení oproti současným gamma kamerám, malé rozměy (velikost USB flash klíčenky) a malá hmotnost (jen 15 g). Především však kamery nevyžadují žádný kolimátor nebo stínění.

Tato práce ukazuje, že detektory čítající jednotlivé fotony, jako například Timepix3, umožňují zásadně zlepšit kvalitu snímků v medicínském zobrazování. Otevírají také nové zobrazovací modality a aplikace.

Klíčová slova: Zobrazování v medicíně, Medipix, Timepix3, SPECT, PET, Compton kamera

List of Abbreviations

APD Avalanche Photo Diode

ASIC Application-specific integrated circuit

BSR Background to Signal Ratio

CAT Computed Axial Tomography

CDR Clock and Data Recovery

CdTe Cadmium telluride

CERN Conseil Européen pour la Recherche Nucléaire

CMOS Complementary Metal-Oxide Semiconductor

CSA Charge Sensitive Amplifier

CT Computed Tomography

CZT Cadmium zinc telluride

DAQ Data Acquisition System

DDR Double Data Rate

EBCT Electron Beam Computed Tomography

FBP Filtered Back Projection

FPD Flat Panel Detector

FSR Fast Shift Register

GaAs Gallium arsenide

HEP High Energy Physics

LOR Line of Response

LSFR Linear-feedback Shift Register

MPI Magnetic Particle Imaging

MRI Magnetic Resonance Imaging

PET Positron Emission Tomography

PMT Photo Multiplier Tube

PSF Point Spread Function

QE Quantum Efficiency

SBR Signal to Background Ratio

SiMP Silicon Photo Multiplier

SLVS Scalable low-voltage signaling

SNR Signal to noise ratio

SPAD Single-photon Avalanche Photo Diode

SPECT Single-Photon Emission Computed Tomograpy

TFT Thin-film Transistor

ToA Time-of-Arrival

ToT Time-over-Threshold

VCO Voltage-controller Oscillator

Contents

1 Introduction

From the ancient times people have been trying to understand why they got ill, what they were suffering from and what they could do to get better. At first, people were seeking answers in spiritual and supernatural world. Later, they realized that the causes of the illnesses were of the natural origin. The first ancient physicians tried to identify the diseases from its signs and symptoms, but they had only limited diagnostics methods, mainly medical history, observation and examination. They were not able to look inside the human body to find out the cause of the illnesses. This has changed with the arrival of the 20th century. There has been a rapid progress in medicine and many new diagnostic methods has been invented. With the discovery of X-rays by Wilhelm Röntgen a new medical field was born - medical imaging that allowed to look inside the human body and thus better diagnose the illnesses.

During the 20th century, many new imaging techniques has been developed for the medical imaging, which nowadays encompasses a wide range of modalities based on different physical principles like ultrasound waves, magnetic fields or ionizing radiation. The quality of the images from these modalities depends significantly on the quality of the used imaging detectors. Looking just at the ionizing radiation applications, there are many types of the detectors available, from old analog devices (e.g. films) to fully digital detectors such as flat panels, that are the most widely used today. The new detectors are being developed and new detection technologies such as photon counting explored. The most recent and state of the art technology being developed is the single photon counting, where the detector is able process each individual photon. The Medipix family of detectors, developed at CERN, are the most advanced hybrid single photon counting pixel detectors available today. They offer high spatial resolution and complex processing logic in each pixel and can be combined with different sensor materials optimized for a particular application. The newest detector of this family, Timepix3, can measure very precisely energy and time of arrival of the incident radiation in each pixel. This makes it a very attractive detector for different medical imaging applications.

The motivation of this thesis is therefore to evaluate the advance properties of the Medipix detectors (especially Timepix3 detector) and to explore the possible application of this detectors in the medical imaging modalities that use ionizing radiation. The first chapter introduces medical imaging and its different methods such as radiography, CT, SPECT or PET. The second chapter describes different types of imaging detectors from the analog devices like X-ray films to digital detectors such as flat-panels or photon counting detectors. The chapter results summaries, in a form of 5 publications, the development of hardware, software, algorithms and methods for Timepix3 detector. Furthermore, it describes the gradual progress of exploring the Timepix3 detector modalities and their applicability in medical imaging.

Firstly, the development of readout hardware and software together with correction and calibration methods is presented. This is a needed first step in order to be able to acquire the physics data from Timepix3 detectors. The functionality of the hardware, software and corrections method together with the Timepix3 counting modality is evaluated in a very fast radiographic measurements. Then, the energy information is exploited for the energy filtering in SPECT applications. The time information is explored in PET application, to find the coincidence gamma events from positron annihilation. Later, both the time and energy information is used to distinguish Compton scattering events in the multi-layer Compton camera application. And, lastly, the very precise timing of Timepix3 (1.6 ns) together with high energy resolution are used for measuring of the depth of interaction in the sensor (by measuring the charge collection time). An unique measurement that was not possible before Timepix3. This depth information is then used for construction of the Compton camera using only a single monolithic Timepix3 detector.

1.1 Research goals

The research goals of the thesis were:

- Exploring the properties and features of the Timepix3 single photon counting detector
- Developing of the readout interface and software for the control and acquisition of the data
- Characterization of the Timepix3 detector
- Developing of correction and calibration methods to obtain physical data
- Developing of methods for energy spectra correction and image quality improvements: suppression of the unwanted effects such as internal XRF; sub pixel resolution, etc.
- Exploring usage of the Timepix3 in different imaging techniques such as SPECT, PET, CT
- Developing new algorithms and methods for Timepix3
- Exploring new imaging modalities

2 Medical Imaging

Medical imaging is a technique that allows us to visualize non surgically the internal structure of the body in order to diagnose or treat medical conditions. It permits also monitoring of physical processes or functions of different organs inside the body (Heidekker, 2013). The term medical imaging encompasses wide range of techniques based on different physical principles:

- Visible light, Near-infrared light - Endoscopy, In vivo microscopic imaging, optical imaging
- Sound waves - Ultrasonography, Photoacoustics (in combination with light)
- Magnetic field - Magnetic Resonance Imaging (MRI), Magnetic Particle Imaging (MPI)
- Radiation - X-rays, Scintigraphy, PET, SPECT, CT, ...

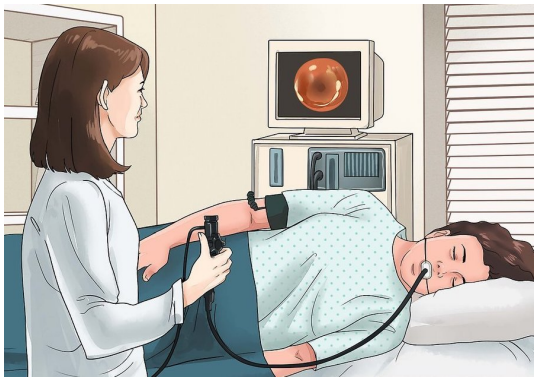

Fig. 2.1: Illustration of an endoscopy examination (Wikihow, 2019).

The visible light applications are imaging techniques that uses small optical instruments to look deep inside the body. The most important visible light techniques is endoscopy that uses an endoscope to look inside cavities in the human body. The endoscopes are flexible tubular instruments equipped with optics and a light source The modern endoscopes use miniaturized cameras that record video which is shown on a monitor. The endoscopy is used in various applications for diagnosis, treatment as well as a helping instrument in surgical interventions. The in vivo microscopy utilizes two-photon or multi-photon microscope to observe structures inside the body with excellent resolution but not very deep (Streba et al., 2018). Optical imaging uses fluorescence or bioluminiscence detection in vivo mainly in preclinical research due to small depth of light penetration (Hani and Kumar, 2017).

The technique using sounds waves (ultrasonography) is a technique based on registering of ultrasound reflected of the tissues inside the body. This diagnostic techniques is capable of imaging internal body parts such as muscles, internal organs or blood vessels. One of the typical application is the examination of pregnant women (see figure 2.2). The method has advantages that is cheaper, more portable than other techniques. It also does not expose patient with harmful radiation. Disadvantages are the limited field of view and difficulties in imaging of structures behind bones (Nakamoto et al., 2015).

The photoacoustics utilizes laser pulses that excite sensitive molecules inside the tissue and cause their thermal expansion that finally converts to a sound wave detected by an ultrasound wave. Again, small light penetration (approx.. 10 mm) predispose this method mostly to preclinical imaging of small animals. In humans, the method can be useful e.g. for melanoma screening (Zou et al., 2016).

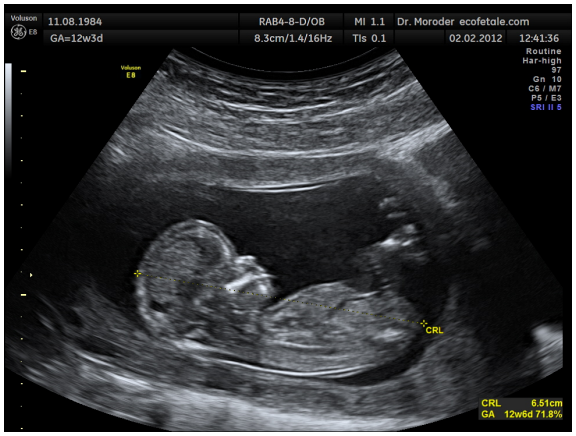

Fig. 2.2: Ultrasound image of a fetus in the womb, viewed at 12 weeks of pregnancy. (Moroder, 2019).

The Magnetic Resonance Imaging (MRI) or Magnetic Particle Imaging (MPI) are techniques that are using properties of magnetic fields. MRI is used for visualization of internal organs and structures in the human body (see figure 2.3). The MRI is using very strong magnetic field (with intensities up to several Tesla) and radio waves with high frequency. The technique is based on magnetic resonance of hydrogen nuclei (protons) of water molecules inside human tissue. These protons are aligned with the direction of the magnetic field and, when high frequency radio waves are passed through a part of the body, the protons move out of alignment. After turning off the radio waves, the protons realign and produce radio signals which are recorded by radio antennas (Weber, 2013). On the other hand, MPI technique is using superparamagnetic iron oxide nanoparticles as tracers purely for molecular imaging without anatomical information. It detects the concentrations of the nanoparticles in parts of the body with high speed, sensitivity and sub-millimeter resolution (Knopp and Buzug, 2012). Both of the magnetic field techniques are non-invasive and do not expose the human body to harmful radiation. However, the machines are more expensive than CT scanners and the case of MRI, the scans usually take much longer.

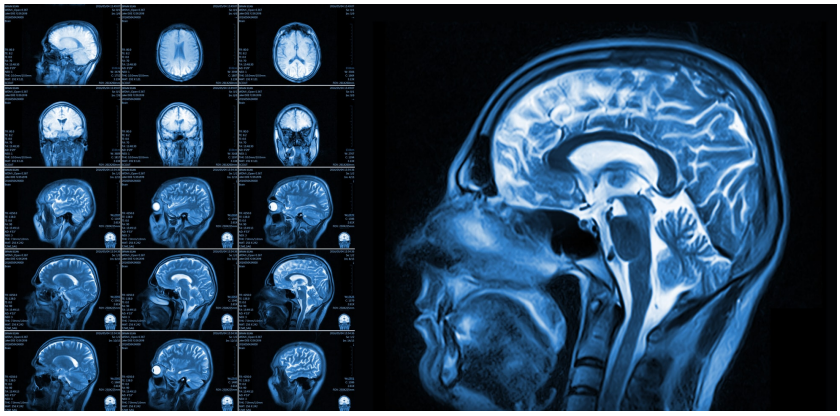

Fig. 2.3: Example of a magnetic resonance image (Radiology, 2019).

The last and the largest group of techniques is composed of the methods that use different forms of ionizing radiation such as X-rays or gamma radiation. Depending on the used technique, one can obtain information about the internal structure (anatomy) of the organs in the human body (their size, volume, location, etc.) or the information about their functioning (their physiology, metabolism, etc.). The first group of methods is called anatomical / structural imaging, the second functional / molecular imaging. The majority of structural imaging methods are based on X-rays. They use an X-ray source (X-ray tube) and a radiation detector (scintillators, photon counting detectors, etc.). The X-ray tube is positioned on one side of the object (e.g. body) and the detector on the other side. The detector records the attenuation of the X-rays that pass through the body (different tissues of the body attenuate differently). The recorded image (projection) then shows these differences in the attenuation as different shades of gray (Martz et al., 2016). More advances techniques like Computer Tomography (CT) can use multiple projections taken from different angles and can create cross-section images or 3D models of the internal structures in the body.

In contrast to anatomical imaging, the functional imaging is examining the radiation emitted from within the body. It usually uses radioactive isotopes attached to a chemical compounds (radio tracers) as the source of the radiation (mostly gamma radiation). These radiotracers are injected into the body and their distribution in the different tissues is observed. The distribution of the tracers depends largely on the metabolism, which can significantly change in the presence of a disease (Luna et al., 2014). For example the cancer cells usually have increased metabolism and therefore accumulate more of the radio tracer. The typical applications of functional imaging are scintigraphy, Single Photon Emission Tomography (SPECT), or Positron Emission Tomography (PET). Each methods uses one or multiple radiation detectors that are positioned around the body and record the emitted radiation.

This chapter will further focus on the imaging methods that are using ionizing radiation and describe some of them in more detail.

2.1 Radiography

Radiography is one of the oldest techniques that uses X-ray or gamma rays to visualize the internal structure of an object. The term covers a wide range of application from medical radiography, where it visualizes the internal parts of a body, to industrial radiography, where the internal structures and defects of objects are examined (Carroll, 2014). The X-rays were discovered by accident in 1895 by German physicist professor Wilhelm Conrad Röntgen. They are form of invisible, highly penetrating, electromagnetic radiation of wave-lengths shorter than UV-rays. They are produced by an X-ray tube and can pass through solid objects. The penetration depends on the density of the material - the higher density material absorbs the X-rays more than less dense materials. The X-ray radiography is based on this principle. To create a radiographic image, the beam of X-rays is generated from X-ray source (usually X-ray tube). The beam passes through the examined object, where part of the beam is attenuated, depending on the density of the object's parts in the beam path. The attenuated beam then exits the object, carrying information about structure of the object in the beam path, and hits the image detector where the projection image is created (see figure 2.4).

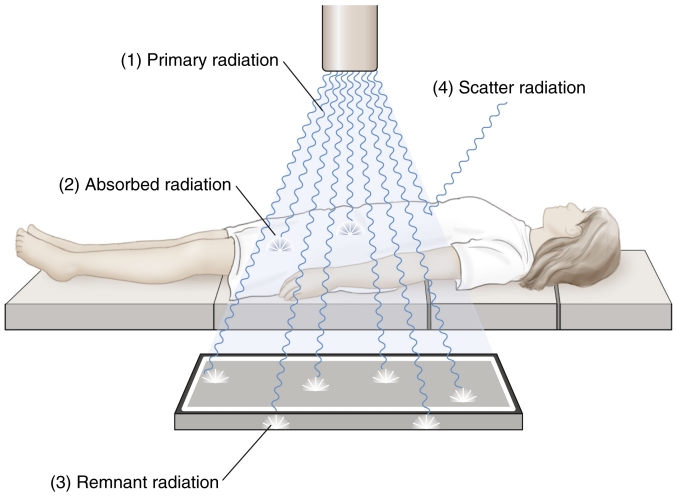

Fig. 2.4: The path and attenuation of a beam of X-radiation.(1) The primary beam exits the x-ray tube. (2) The beam enters the patient, where the individual x-ray photons' energies are altered (attenuated) by their passage through body tissues of varying characteristics. (3) The attenuated, or remnant, beam exits the patient, carrying with it an energy representation of the body tissues traversed and strike the image receptor. (4) Some x-ray photons interact with matter and continue in a different direction, producing scatter radiation, which is nondiagnostic(Adler and Carlton, 2016).

The projection image is basically a "shadow" image of the remnant beam after passing through the object. The lighter colors in the gray scale image shows parts of the object with higher density (more of the beam was absorbed) and the darker colors parts with less density. An example of such a projection image is shown in figure 2.5 - an image of can of sardines. The bones and the can have higher density (better contrast) than the soft tissue of the fish.

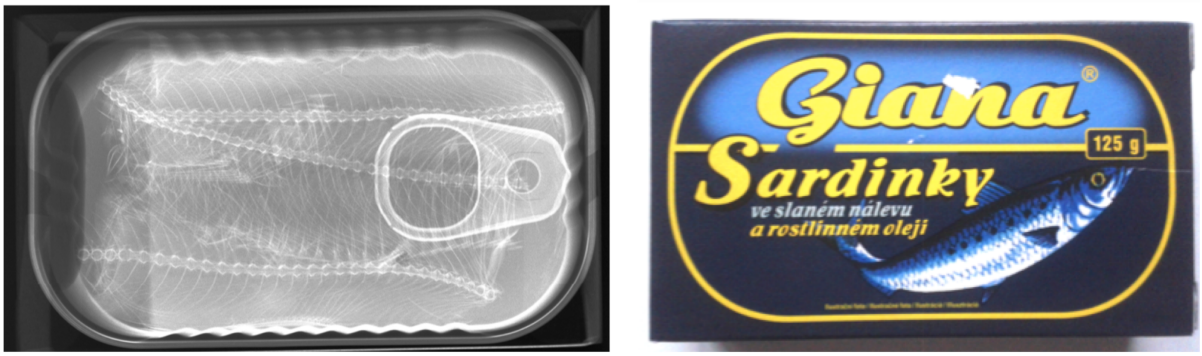

Fig. 2.5: Example of an X-ray radiography image - can of sardines. X-ray image (left), Photo of the can of sardines in a paper box (right). The X-ray image shows very fine structure of fish bones as well as the paper box.

The imaging detector can be of different types. The first detector used for radiography was a photographic plate. It was a glass plate with light sensitive emulsion of silver salts. Later they were replaced by a photographic film - a sheet of plastic film base containing small light sensitive silver halide crystals. Nowadays the films were replaced by digital detectors such as imaging plates or flat-panel detectors (Thomas and Banerjee, 2013).

2.1.1 X-Ray generation

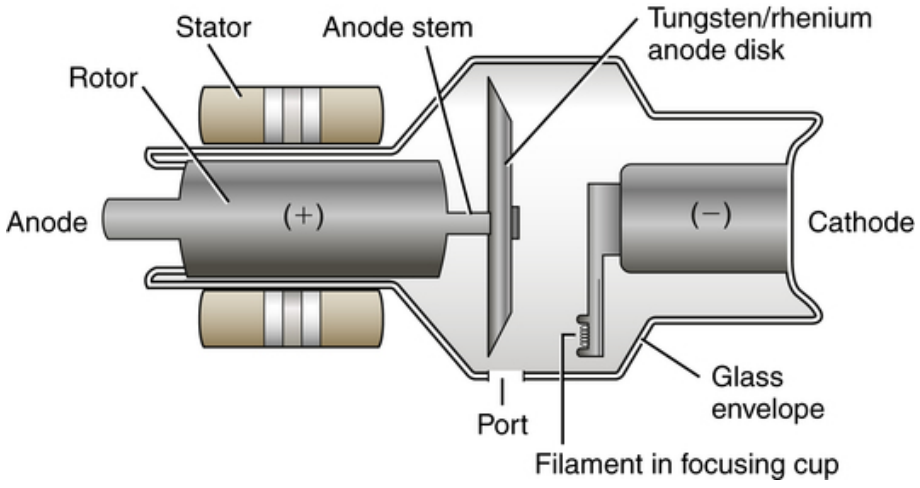

Fig. 2.6: Parts of the X-ray Tube. A cross-sectional view of a basic rotating anode x-ray tube (Johnston and Fauber., 2016).

X-rays are usually generated by an X-ray tube, which is a device that converts electrical power into X-rays (Behling, 2015). The X-ray tube is a vacuum tube that contains two electrodes - anode and cathode (see figure 2.6). The tube is connected to a high voltage power source (25 - 600 kV). The cathode emits electrons that are collected by the anode. When the electrons collide with the anode material (usually tungsten, molybdenum or copper), they decelerate and the X-rays are generated. Only about 1 % of the energy of electrons is converted to X-rays,

the rest is converted to heat. This generated heat has to be removed, otherwise the anode would be evaporated. There are several types of X-ray tube constructions that remove heat in different ways. Some X-ray tubes have a simple construction with a static anode, which is cooled e.g. by water. The other popular construction is a rotating anode tube - the anode consists of a rotation disk connected to a motor. By rotating the anode, the heat is dissipated to a larger surface (Cervantes, 2016).

The X-rays generated from the X-ray tube can actually consist of two different types of radiation: the braking radiation (Bremsstralung) and characteristic X-ray of the the anode target material. The braking radiation is caused by the deceleration of the electrons and has a continuous energy spectrum - the photon energy ranges from 0 to the energy of the electrons. The characteristic X-ray is emitted when a photon collides with the atoms of the anode target. When a photon collides with the atom, it kicks an electron from the atom's electron shell and a vacancy is created. This vacancy is filled by another electron in the atom and an X-ray photon of a specific energy (a characteristic X-ray) is emitted. In opposite to braking radiation, the characteristic X-ray spectrum is discrete. The resulting X-ray spectrum generated from the X-ray tube is a combination of both type of radiations. The figure 2.7 shows a spectrum from an X-ray tube with tungsten target (Als-Nielsen and McMorrow, 2011).

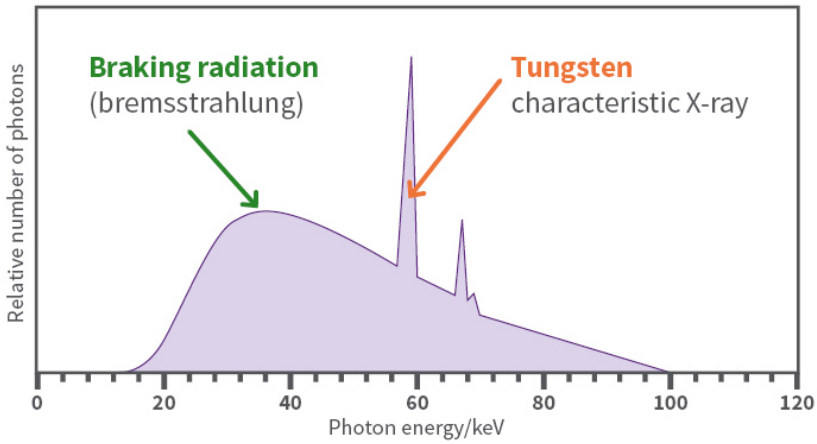

Fig. 2.7: Calculated X-ray spectrum, 100 kV, tungsten target (ARPANSA, 2019).

2.2 Scintigraphy

Scintigraphy is a diagnostic method used in nuclear medicine that produces a functional 2D image. The scintigraphy is in a way very similar to X-ray radiography, but instead of an external radiation source (X-ray tube) it records the radiation emitting from within of the body. Moreover, it does not concentrate on imaging the anatomy, but physiological function of the imaged system. The principle of the scintigraphy is that a patient is given (usually injected into vein) a small amount of a radioactive substance - radioisotopes attached to a drug (radiopharmaceutical) that emits gamma radiation. These drugs are designed to travel into a specific organ or part of the body, where they accumulate. The radiation emitted from the

radiopharmaceuticals (also called radiotracers) is detected by an external gamma detector (usually a gamma camera). Example of a scintigraphy, a bone scan, is shown in figure 2.8.

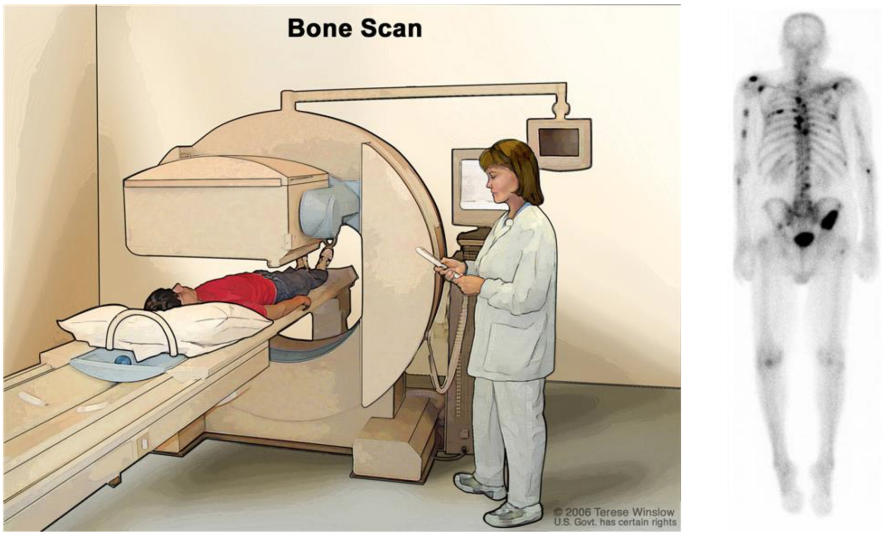

Fig. 2.8: Bone scan. A small amount of radioactive material is injected into the patient's bloodstream and collected in abnormal cells in the bones. As the patient lies on a table that slides under the scanner, the radioactive material is detected and images are made on a computer screen or film (left). (National Cancer Institute, 2019) Bone scan showing multiple bone metastases from prostate cancer (right). (Wikipedia, 2019).

The scintigraphy can be used in several different modalities:

- Static acquisition - detector is in a fixed position relative to the body. Used for example for examination of thyroid gland, kidney, etc.

- Scanning of the whole body - the detector or patient moves resulting in full-body scan of the patient from head to foot creating one large image. Typical application is a bone scan.

- Dynamic acquisition as a function of time - the detector scans one area of the body making a video that is used to study some important dynamic biological processes. Typical applications are scintigraphy of the heart ventricle, kidney or bone phase's vascular scan.

2.3 Computed Tomography

Computed Tomography (CT), sometimes also called computed axial tomography (CAT), is a radiologic diagnostic method that, with help of X-rays, allows noninvasive imaging of internal parts of the human body or other objects with high resolution. The CT is used in clinical medicine or preclinical studies on small animals, but also in industry to inspect defects or internal structures of different objects and materials. The CT was introduced in 1971 by

Cormack and Hounsfield. It is the first imaging modality where the Computer is required to reconstruct images (Heidekker, 2013). Figure 2.9 shows an example of a CT scanner.

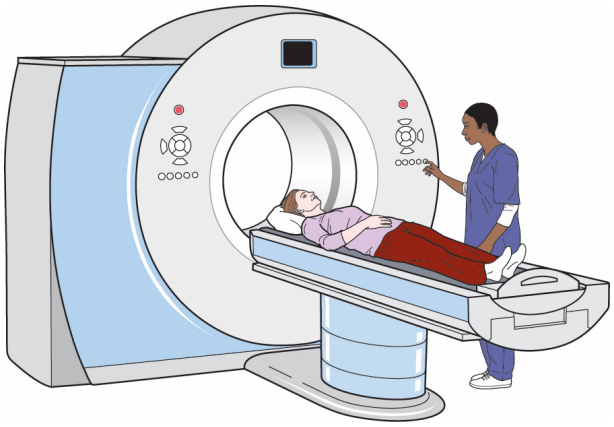

Fig. 2.9: A person having a CT scan (Macmilian, 2019)

In the traditional radiography, an object is irradiated by X-rays and the projection image is recorded on a film or detector. The resulting image is a projection of the body's volume on a 2D plane. Different parts of the body, that overlaps in the beam path, are projected in the same image. It is then impossible to distinguish if the lighter area in the image is a material with higher absorption or if it is because of the higher summation thickness of different parts in the body.

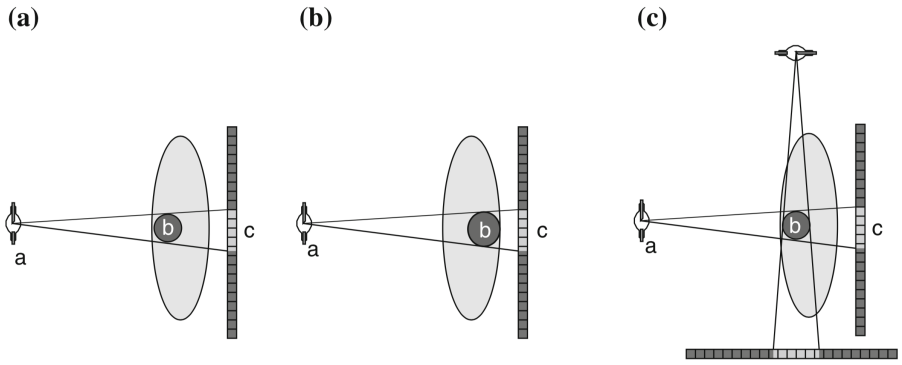

Fig. 2.10: Ambiguity in an X-ray projection. The projection image is very similar in cases a and b, although the position of the tumor is very different. c Some of the ambiguity can be removed by taking two perpendicular X-ray images. (Heidekker, 2013)

Moreover, it is also not possible to determine precise position of the examined part of the body in projection axis (see figure 2.10). Therefore, 2D radiography is sometimes not sufficient to visualize details of some structures in the body.

In the computed tomography, many 2D projection images from different angles are taken and then, with the help of a computer, a cross-section images (slices) are reconstructed. From these slices a 3D model of the object can be created. Compared to simple radiography, the

reconstructed slices offer higher contrast and more information about the inner structure of the object.

2.3.1 Principle of the computed tomography

The conventional CT scanner (third generation) consist of a X-ray tube and a detector placed opposite to each other on a rotating ring (see figure 2.14). The X-ray tube and the detectors rotate around the object (patient) in a plane perpendicular to the length axis of the patient and make 1D transmission images of a section of the object, recording the absorption profiles from different angles (see figure 2.11). Modern CT scanner can record several sections of the object at the same time (Kalender, 2011).

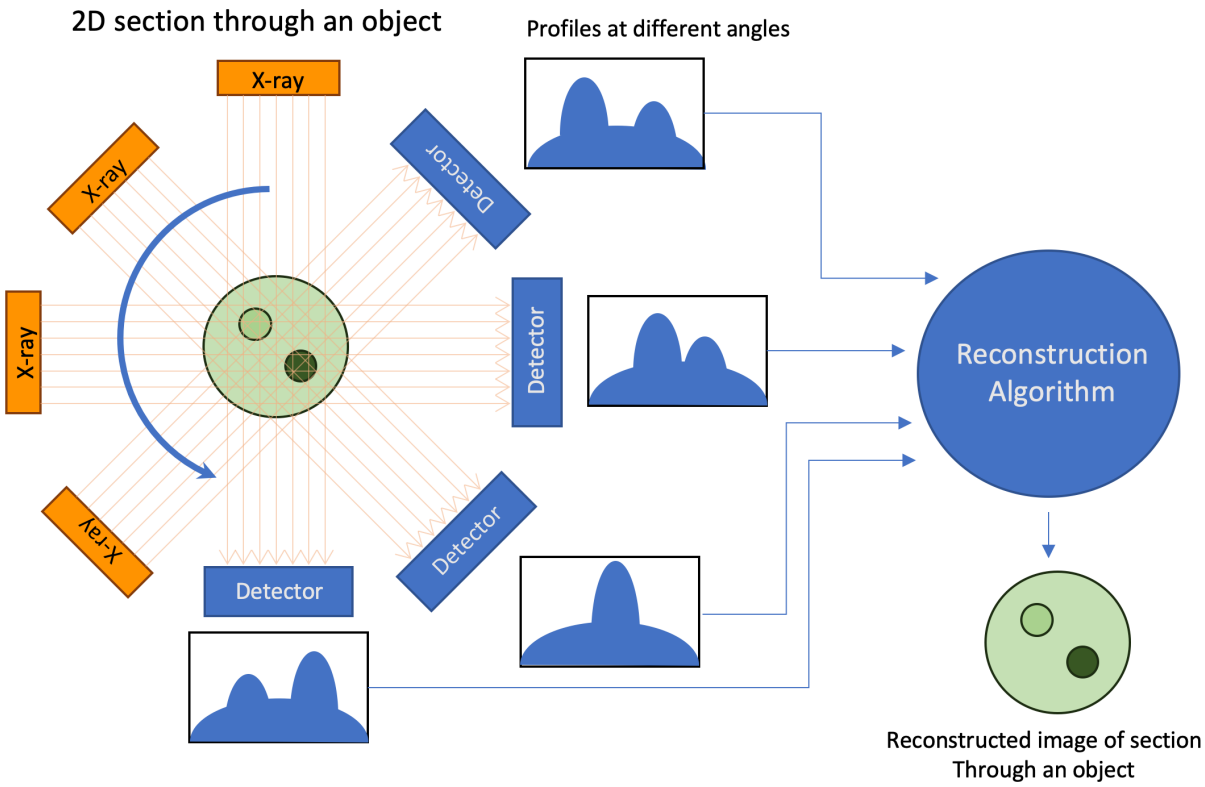

Fig. 2.11: Schema of the tomography principle. By rotating the X-ray and detector around the object several one dimensional absorption profiles are recorded. They are processed by the reconstruction algorithm to obtain image of the object section.

The absorption profiles taken at different angles for the full revolution of the scanner are assembled into one image called sinogram (see figure 2.12). From this image a section of the object can be reconstructed. There are mainly two methods used for reconstruction nowadays: filtered back projection (FBP) or iterative method.

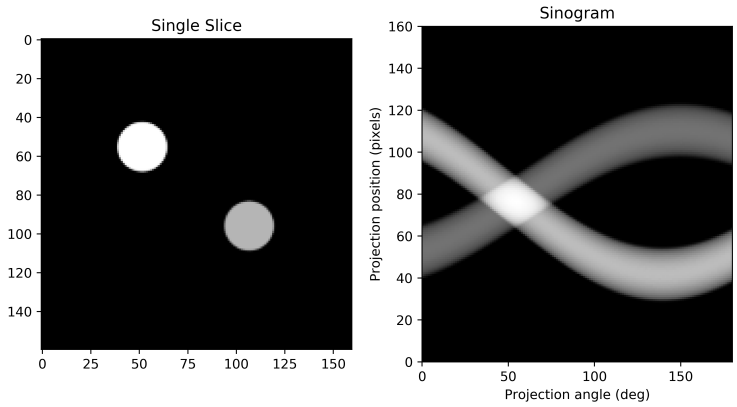

Fig. 2.12: Image of a section of an object (left) and its corresponding sinogram - absorption profiles for angles from 0 - 180 degrees (right).

Filtered Back Projection

Back projection is a method to reconstruct the original absorption at different places inside the object. Each pixel of the measured absorption profile represent a summation absorption along the line. Since the values of the absorption in each point along the line are lost, a constant value (the summation absorption from the profile) is projected along the line (see figure 2.13). By projecting multiple angles the shape of the object can be reconstructed, however with decrease quality and many artifacts. To improve the quality of the reconstructed image, the measured data are filtered before they are back projected, usually by ramp and low-pass filters. The FBP works reasonably fast and is easy to implement, however, it requires large number of projections and full range of angles. Moreover, the image quality decreases rapidly with the amount of noise in the measured data (Romans, 2011).

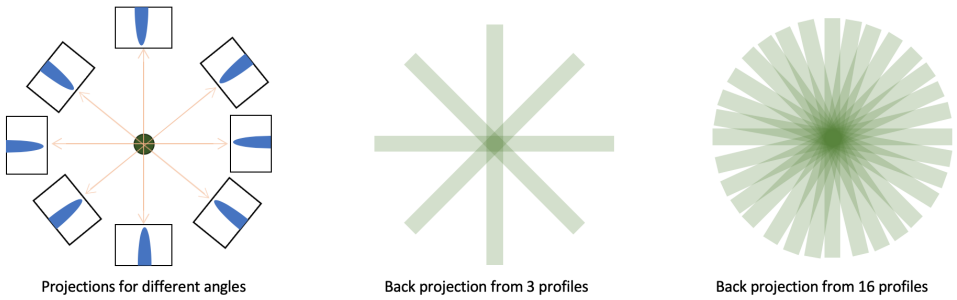

Fig. 2.13: Example of back projection of a point. Measured absorption profiles (left). Back projection only from 3 profiles (middle). Back projection from 16 profiles.

Iterative Image Reconstruction

The iterative methods are based on the continuous improvement of a model of the object so that the best agreement between the measured projections and projections created from the model is reached. First, an initial guess of the model is calculated (e.g. just using simple back projection). Then, the forward projection of the model is created and compared with the measured data. The correction of the model is calculated and the corrected model is again forward projected. This is repeated until a convergence is reached. The advantages of the iterative methods is that the convergence is relatively fast, stable and that it is possible to implement more complex geometries and include very complex physics models. The disadvantage is the computational complexity (Zeng, 2010).

2.3.2 Generations of CT scanners

The conventional CT scanners nowadays look quite different from the early devices. Over the years several generations of CT scanners were developed to increase efficiency of the scanning. The differences between the generations are mostly in arrangement of the X-ray tube and the detector. (see figure 2.14).

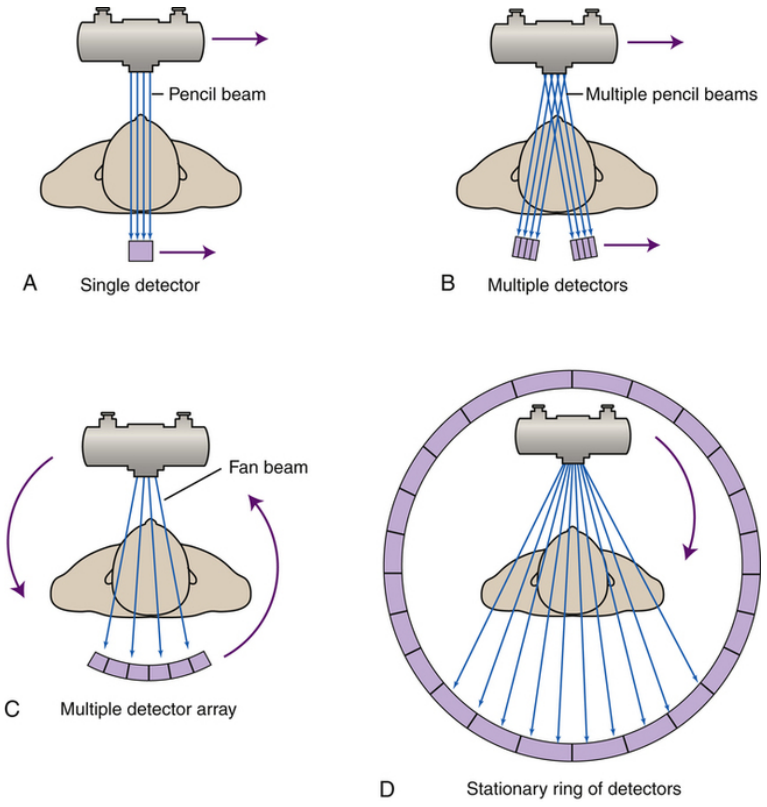

Fig. 2.14: The first four generations of computed tomography scanning methods (first generation [A], second generation [B], third generation [C], and fourth generation [D]) demonstrate how changes in the tube movement and detector configuration have evolved. (Johnston and Fauber., 2016)

There are several generations of CT systems (Cantatore and Muller, 2011):

- **First generation** systems used single X-ray source (a pencil beam) and single detector. The X-ray beam moved linearly over the patient and the detector followed. After each linear scan the X-ray tube and the detector rotated. The major disadvantage of this system were long scanning times. It is no longer used today.

- **Second generation** systems were very similar to first generation. The only difference was usage of a fan beam (but not with full field of view) instead of the thin pencil beam and multiple detectors. This system is also not used today.

- **Third generation** systems used wider fan beam that covered the entire field of view, therefore the translation was no longer necessary. The systems were faster and used larger amount of sensors in the detector array. This is the basis for the current CT systems.

- **Fourth generation** systems also use only rotation movement. The system consists of single X-ray source and stationary ring with multiple detectors. Only the X-ray source rotates. This design was later abandoned due to high cost and problems with scatter artifacts.

- **Fifth generation** systems, also called electron beam imaging (EBCT) systems, do not use any motion in contrast to previous systems. The electron beam is generated outside of the gantry. The gantry is divided into halfs - one half are detectors and the second half tungsten targets that are bombarded by an electron beam. These systems are very fast and used mostly for cardiac imaging.

- **Sixth generation** systems allows for continuous scanning. The limitation of the previous systems was that they had to stop after complete revolution and return to the starting position (because of wire connection). The sixth generation systems use slip ring technology that allows electrical signal to pass to rotating parts without need for stationary components. This allowed helical movement of the scanners and faster scanning times.

- **Seventh generation** systems feature multiple detector array and a cone shaped beam. The cone beam does not pass through a narrow collimator, therefore the intensity of the X-ray beam is not that strongly reduced and can be efficiently used.

2.4 Single-Photon Emission Computed Tomography (SPECT)

Single-Photon Emission Computed Tomography (SPECT) is a nuclear medicine tomographic imaging technique using gamma rays. It is an extension of planar scintigraphy imaging producing cross-sectional or three-dimensional images of physiological activity in the body. An example of SPECT scanner (GE Optima NM/CT 640) is shown in figure 2.15.

Fig. 2.15: SPECT Scanner GE Optima NM/CT 640 (GE, 2019).

Before the SPECT scan, the patient is given (usually intravenously) a radiopharmaceutical that is targeted to the examined tissue / organ. The radiopharmaceutical is emitting gamma rays mostly in energy range of 80 to 300 keV that are detected by the gamma camera (Heidekker, 2013). One or multiple gamma cameras rotate around the patient and detect the gamma rays from different angles (see figure 2.16). The measured projection can be reconstructed similarly as in the case of computed tomography. The result of reconstruction can be 2D cross-section images or 3D model that visualizes the distribution of the radiopharmaceutical in the body. The most commonly used radiopharmaceuticals contain gamma-emitting radionuclides such as ^{99m}Tc (140.5 keV), ^{67}Ga (93Kev, 185 keV and 300 keV), ^{111}In (171.3 keV and 245.4 keV) or ^{123}I (159 keV) (Vallabhajosula, 2009).

The gamma camera construction usually consists of a collimator, scintillator crystals and photo multiplier tubes (see figure 2.16). The collimator consists of a thick sheet of lead (25 - 75 mm) with multiple holes. Only the photons passing the collimator holes can be detected by the scintillator in order to obtain spatial information of the gammas emitted from the body. The collimator attenuates more than 99 % of the incident photons and therefore limits the camera sensitivity. To improve the sensitivity the gamma camera has to be placed as close

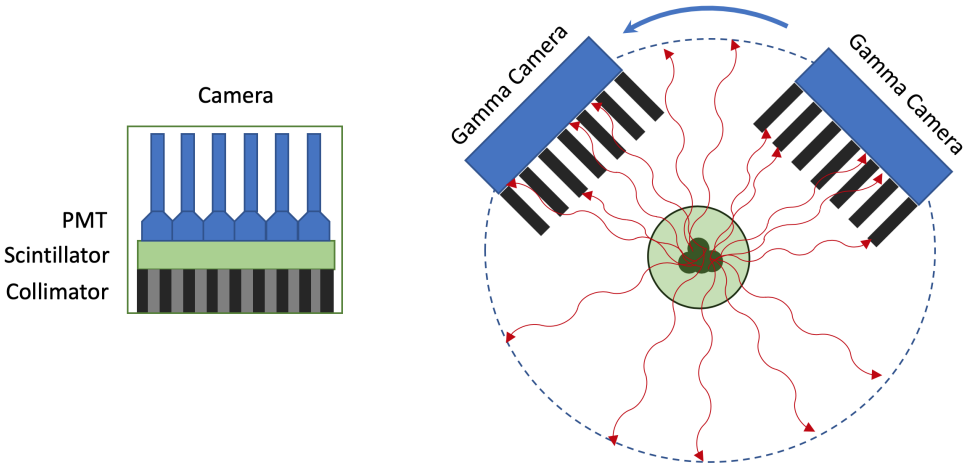

Fig. 2.16: Schema of SPECT gamma camera (left). Schematic of SPECT scanning. Most of the gamma photons are attenuated by the collimator (right).

as possible to the patient. The image quality increases also with higher acquired statistics. However, the acquisition time is usually limited by the comfort of the patient. Typically, the time for a single projection is between 15 - 20 seconds, giving the total scanning time of 15 to 20 minutes (Lawson et al., 2013).

The modern systems often combine functional images from SPECT with anatomical images from CT in a single device (called SPECT/CT). The combination of both modalities enables direct correlation of the anatomic and functional information. It improves localization of e.g. tumors recorded by SPECT, thus improving diagnostic possibilities in many clinical applications. Furthermore, it simplifies the complex examination of patients, where two separate systems had to be used in the past, and reduces the examination time. It is also more cost effective.

2.5 Positron Emission Tomography (PET)

Positron Emission Tomography (PET) is a nuclear medicine functional technique used for examining of metabolic activity in the body and diagnosis of diseases. It is based on the detection of pairs of gamma rays emitted from the patient's body after an annihilation of positrons and electrons. The positrons are emitted by a radiopharmaceutical (a biologically active molecules labelled with a radioactive tracer) that is injected into the body. The most common tracer for PET is fluorodeoxyglucose (^{18}F FDG) that is used mainly for diagnosis of cancer. The FDG is an analog of glucose and it can indicate regions of increased metabolic activity (higher glucose uptake) caused by cancer tissue. PET is again not only used in clinical oncology, but also in preclinical studies on animals (e.g. mice) (Sharp et al., 2005).

2.5.1 Principle of PET

The PET is based on the same principles as scintigraphy. The patients is injected with a radiopharmaceutical that contains radionuclides emitting positrons (β^+ radiation). Such an emitted positron travels a very short distance in the body before it collides with an electron. When the electron and positron collide they annihilate into two 511 keV gamma photons that travel in the opposite directions (180° apart) along the line (see 2.17) (Granov et al., 2013).

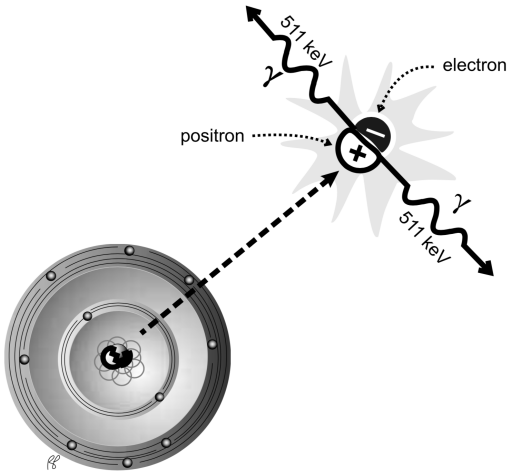

Fig. 2.17: Annihilation of en electron and positron (Powsner and Powsner, 2006).

The gamma photons are detected by the ring of detectors around the patient (see figure 2.18), that work in a coincidence mode. It means, that only the gamma photons that are detected at same time (in coincidence) are recorded. This principle not only reduces the noise, but also helps in reconstruction of the annihilation origin. This origin lies on an imaginary line (called line of response LOR) that can be drawn between each two detectors in opposite sides that detected a coincidence events. From larger number of these lines, a distribution of the radiopharmaceutical in the patient's body can be reconstructed (see figure 2.18).

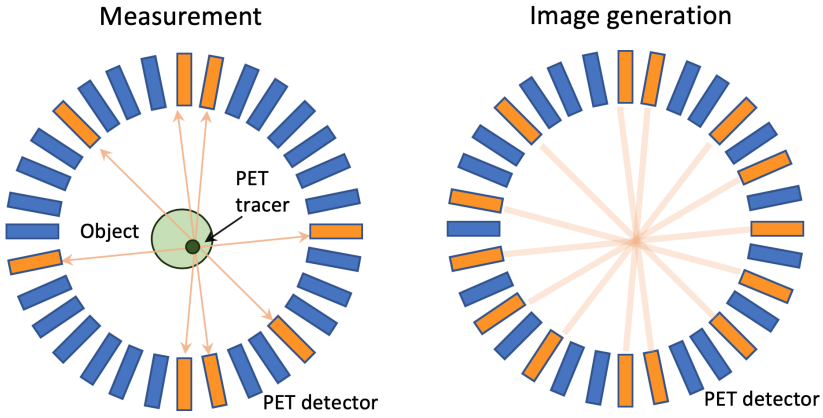

Fig. 2.18: PET measurement and image generation.

Although a significant part of the noise can be suppressed thanks to the coincidence technique, there is a possibility of false coincidence events. One type of the false events can for example arise from two annihilation events, where only one event from each pair is detected and are mistakenly assigned to the same coincidence event. The other false coincidences can be caused by detection of non-annihilation photons. Furthermore, some of the annihilation photons can be scattered in the body and their path altered. In the reconstruction, they are then incorrectly presumed to be on the line between the two detectors. The probability of the false coincidences increases with the increase of radioactivity. Therefore, this represents a problem with higher count rates. (Powsner and Powsner, 2006).

Time of flight technique

Time of flight is a technique that can improve the resolution of the PET scanner. Because the annihilation occurs in different places inside the detection ring, one of the coincidence photons arrives before the other. The difference in the time of arrival of the two events is proportional to the distance traveled and therefore can be used to calculate the position of the annihilation on the line between the detectors. However, the available detectors and electronics are not yet precise enough and therefore this method can reduce the spatial resolution. Nevertheless, it is a promising method for the future.

2.5.2 PET Systems

The PET systems, in comparison to SPECT, have the advantage that they do not need a collimator and therefore can offer higher sensitivity. However, their major limitation is to achieve a good temporal resolution. Especially in high data rates it can be a problem to suppress false coincidence events.

The conventional PET system consists of the ring of detectors, mostly scintillators with photo multiplier tubes (PMT). The used scintillation crystal is a crucial parameter of the whole system. There are several different materials that were used for PET over the years. The most often used crystal up until recently was Bismuth germanante (BGO), which has a high density (stopping power) but relatively low light output. The latest generation of the PET systems use lutetion orthosilicate (LSO) crystals or gadolinium orthosilicate (GSO). These have shorter decay time and high light output (Sharp et al., 2005).

Block Detectors

To improve the spatial resolution of the PET detectors the block detectors are used. The block detector consists of a single crystal divided into an array of smaller elements (typically 8x8,

with a size of 3 mm to 6.5 mm) each connected to its own photo multiplier tube (see figure 2.19). The blocks are grouped into cassettes and these are then arranged into one or multiple rings around the patient.

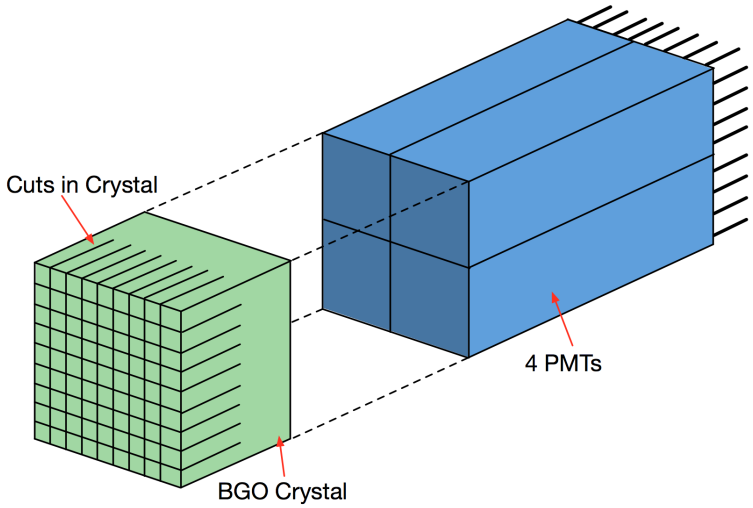

Fig. 2.19: A schematic of PET detector block (Binns, 2001), edited.

Timing Resolution

From the principle of PET the gamma photons should be detected at the same time. However, in reality each photon can arrive at the opposite detectors at a slightly different time. This uncertainty of the time detection is called a timing resolution (time coincidence window) of the detector. The time difference can be caused by several effects. First, the annihilation can occur closed to one the of the detectors and second, the delay can be caused by the variations of the electronics and scintillations crystal at each detector. For the full-body PET scanner with a diameter of 1 m the time difference between the photons (based on the travelled length) can be of about 3 to 4 ns. Therefore, the typical coincidence window of PET scanners are between 6 to 20 ns (Saha, 2006).

Modern PET Systems

Similarly, as in the case of SPECT systems, a combined PET/CT systems have been developed that permit a fusion of function PET images with anatomical images from CT scanners. In this combined system both detectors are placed on the gantry, where in contrast to SPECT, the PET detector is placed behind the CT detector. This fusion of PET and CT provides more accurate images that help with diagnosis of various human diseases. It also reduces the scanning times. More recently, use of nonmagnetic materials allowed to combine PET and MRI into one device which allowed to significantly decrease a radiation dose absorbed by a patient and also brought more anatomical information in terms of soft tissues (Zaidi and Kwee, 2013).

3 Imaging Detectors

The quality of the data and images in all the medical imaging applications depends significantly on the parameters of the imaging detectors. There is a large variety of the detector types, each based on different physical principles (Cerrito, 2018). The oldest types were pure analog devices using glass plates or films with an chemical emulsion sensitive to radiation. To obtain a permanent image they had to be processed and developed. More recent types of detectors are based on scintillators that convert radiation to visible light, which is then recorded by a photo detector (e.g. photo multiplier tube). The modern imaging detectors such as flat panels are fully digital and convert the radiation directly into electrical signal. The latest generation of the detectors is using single photon counting technology that allows counting and processing of each single photon.

3.1 Scintillation Detectors

Scintillation detectors are one of the oldest types of detectors used to record ionizing radiation. They consist of a scintillator and photon (visible light) detector. The scintillator is usually a crystal material that can absorb ionizing radiation and emit a small flash of light, a scintillation. Early scintillation detectors were just scintillators where the flashes of lights were observed and counted by a human eye. Later the first images were recorded when the scintillator was combined with a photographic film. Nowadays, a typical modern scintillation detector (also called scintillation counter) consists of two parts - a scintillator that converts the incident radiation into visible light and a sensitive light detector that detects the visible light, amplifies it and converts it to electrical pulses that can be processed by readout electronics and a computer. The light detectors can be in a form of photomultiplier tubes (PMT), photodiodes, micro-channel plates or silicon photomultipliers (SiMPs) (Waterstram-Rich and Gilmore, 2016).

The scintillators can be made from different materials. The are several commonly used types of scintillation material - inorganic crystal, organic crystals, organic-based liquids, and plastics. Each material has different properties, advantages and disadvantages. The ideal scintillator should have a high scintillation efficiency, linearity, high transparency for the emitted light wavelengths, fast decay time and small index of refraction. None of the scintillation material fulfills perfectly all these criteria. Therefore, choosing the proper material for the particular application is always a compromise (Korzhik and Gektin, 2017).

3.1.1 Scintillators

Inorganic Scintillators

Inorganic scintillators are usually made from inorganic alkali halides crystals. The scintillation mechanism in these crystal depends on the structure of the crystal lattice. Some crystal can scintillate directly in pure form, whereas another crystal needs an addition of a dopant ion to scintillate. Typical dopants ions are for example thallium (Tl) or cerium (Ce). The most common inorganic scintillators are sodium iodide NaI(Tl) and cesium iodide CsI(Tl), both doped with thallium (Knoll, 2000).

The main advantage of inorganic scintillators is their higher Z and density, resulting in great stopping power. They have also high light output and therefore better energy resolution. This makes them suitable for detection of X-rays, gamma rays or high energy particles. Significant disadvantages are slower time response (in order of 100 ns) and their hygroscopicity - they need to be enclosed tightly to avoid contact with humidity in the air.

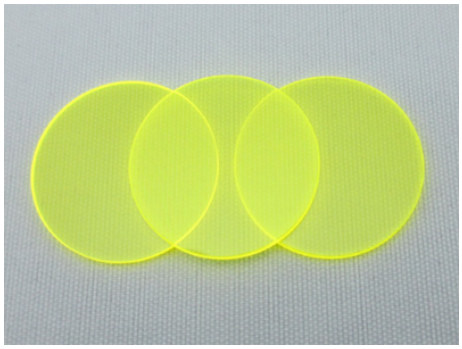

Fig. 3.1: Photo of an inorganic scintillator (Blue-Optics, 2019).

Organic Scintillators

The scintillation principle of organic scintillators is quite different from the inorganic scintillators - it is caused by a transition of electrons to different energy levels in a single molecule. There are 3 types of organic scintillators - organic crystals, organic liquids and plastic scintillators. The organic crystals usually consist of just single component. Their fluorescence time is quite fast (order of nanoseconds). They are mechanically strong, but have anisotropic light output and are difficult to fabricate into desired shape (Horrocks, 2012).

The organic liquids can be a mixture of different crystals in an organic solvent. They offer fast fluorescence time (3 - 4 ns) and can be easily cut into any shape. They can be also mixed with other additives to improve performance (e.g. wavelengths shifters). Their disadvantage is a high sensitivity to impurities.

The plastic scintillators are broadly used in particle and nuclear physics. They are fabricated by dissolving the organic scintillator in a transparent polymer substrate. The most often used polymer bases are aromatic plastics such as polyvinyl-toluene (PVT) or polystyrene (PS). The main advantage of these scintillators is that their production is very cheap and they can be easily modeled into any desired shape. They also offer high light output and very fast response time (2 - 3 ns). Their disadvantage is that they are not very radiation-resistant.

3.1.2 Photo Detectors

Photomultiplier Tube

Photomultiplier tube (PMT) is a very sensitive detector of light in the visible, ultraviolet and near-infrared range of the electromagnetic spectrum. It consists of a vacuum tube that contains a photocathode, several dynodes and a single anode (see figure 3.2). The incident photons are intercepted by the photocathode that is made from thin metal or semiconductor layer deposited on the entrance window of the detector. As a result of the photoelectric effect, electrons are emitted from the surface. These electrons are then focused by the focusing grid of electrodes towards the electron multiplier. The multiplier consists of several dynodes whose aim is to transform the initial photoelectron into emission of more electrons. Typically single dynode as a response to an incident electron emits between two to five electrons (Flyckt, 2002). This way electrons from each dynode are multiplied in the following dynode. The resulting large number of electrons is collected by the anode, where a sharp current pulse is created that can be detected and processed by the electronics, usually an amplifier and discriminator.

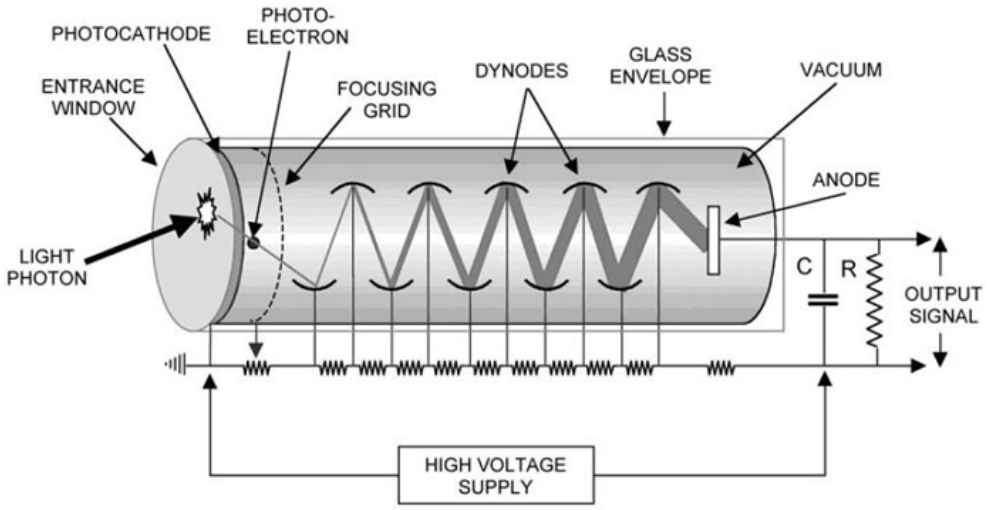

Fig. 3.2: Schema of the photomultiplier tube (PMT) (SENSE, 2019)

The main feature of photomultiplier tubes is that their response is linear - the output voltage of the tube is directly proportional to the energy deposited by the radiation. This linearity is valid for a wide range of amplitudes. The amplification gains of PMT is typically in the range of 10^4

- 10^7. The other important aspect of PMT is that they retain the original timing information of the light pulse - for a short light pulse, a corresponding electron pulse is generated with a delay time of 20 - 50 ns (Knoll, 2000). A disadvantage of the PMT is a sensitivity to magnetic fields - they need to be shielded by a layer of soft iron or mu-metal[1]. Another disadvantage of the PMT is the requirement of high voltage supply (up to 1000 V) needed for the chain of dynodes.

An important parameter characterizing the photomultiplier tubes is the quantum efficiency (QE) of its photocathode. Quantum efficiency describes the photoemission of the cathode and it is defined as the ratio between the number of photoelectrons emitted by the cathode to the number of the incident photons. It is usually expressed as a percentage and is strongly dependent on the wavelength of the incident light. The average quantum efficiency is about 20 - 35 %.

Photodiodes

Photodiodes are an alternative way of detecting light from scintillators. They are semiconductor devices that consist of a thin layer of silicon with a p-n junction or PIN[2] structure. The principle of the photodiode is based on the internal photoelectric effect. When the light is incident on the p-n junction in the photodiode, it generates an electron-hole pair. Because of the built-in electric field of the depletion region, the created free holes and electrons are transported towards the cathode and anode respectively, thus producing an electric current. The advantages of photodiodes are their compact size, higher quantum efficiency (compared to PMT), stability, low power consumption and insensitivity to magnetic fields. Thanks to the small dimensions, the transport of the free carriers is very fast and therefore the time response is comparable to the conventional PMTs. There are two types of photodiode designs used with scintillators - conventional photodiodes and avalanche photodiodes (Yun, 2012).

The conventional photodiodes convert directly photons to electron-hole pairs without an internal gain. Their quantum efficiency is much higher than that of the PMTs (about 60 - 80%) and spans wider range of wavelengths. However, because of no amplification, the output signal is relatively small and the electronic noise poses a significant problem.

The avalanche photodiodes (APD), on the other hand, can amplify the current thanks to the avalanche effect. The diodes are reverse biased with a high voltage (100 - 200 V for silicon) that accelerates the charge carries to such a speed that the collision with the crystal lattice causes a generation of a new electron-hole pair. This pair is also accelerated and generates another new electron-hole pair. In such a chain reaction more and more new pairs are generated, creating an

[1] mu-metal is a nickel-iron soft ferromagnetic alloy with very high permeability, perfect for shielding of sensitive electronics.

[2] PIN - is a structure where the undoped intrinsic semiconductor is surrounded by p-type and n-type semiconductor regions.

avalanche effect. This way, even a single photon can create an ionization of the crystal lattice, resulting in the avalanche effect. In such a case, the diode is called a single-photon avalanche diode (SPAD). The avalanche effect can produce gain factors up to several hundred and thanks to this, the avalanche photodiodes have smaller electronic noise and allow for good energy resolution even for lower radiation energies. The gain is however sensitive to temperature and biasing voltage. Therefore, the avalanche diodes require properly regulated high voltage power supplies (Russell and Cohn, 2012). The main application of the APDs is in the situations where the signal is too high for photomultiplier tube or too small for a conventional photodiode.

Silicon Photomultipliers

Silicon photomultiplier (Semiconductor, 2018) (SiMP) is a device constructed from a grid of many small microcells of single-photon avalanche diodes. The size of each SPAD microcell can be from 10 to 100 micrometers and the density of the microcells could be between 100 and several 1000 per mm^2. In the functionality, they are analogous to photomultiplier tubes. The advantages of the SiMP over PMTs are high gain mode (10^5 - 10^7), low bias voltage (about 50 V), low power consumption, compact size, insensitivity to magnetic fields and radiation hardness. Moreover, they are relatively cheap to produce. The disadvantage is a relatively high dark count (noise) (Feege, 2008).

3.2 Flat-Panel Detectors

The flat-panel detector (FPD) is a modern, relatively thin X-ray detector that instantaneously records digital radiographic images (E. Kotter, 2002). The FPDs consist of a large number of imaging elements (pixels) forming a large matrix (2000 by 2000 or more pixels). The intensity of the electrical signal in the pixel is directly proportional to the intensity of the incident radiation. The flat-panel detector consists of several layers (see figure 3.3). The bottom layer is a glass substrate, in the middle layer is charge readout electronics - a matrix of thin-film transistors (TFT) and the top layer is formed, depending on the type of the flat-panel, by X-ray sensitive or photosensitive detector. X-ray sensitive flat panels are called direct conversion detectors - they use a photoconductor as X-ray detector. The photosensitive flat-panels are called indirect conversion detectors as they use light-sensitive photodiode and scintillators.

Indirect conversion detectors

The top part of the indirect conversion detector is made of a thin layer of scintillation material (usually gadolinium oxysulfide or cesium iodine) that converts radiation into light. Underneath the scintillator is a photodiode that converts light into an electrical charge, which is stored in a capacitor and converted by a matrix of TFT into a digital signal. The bottom part of the

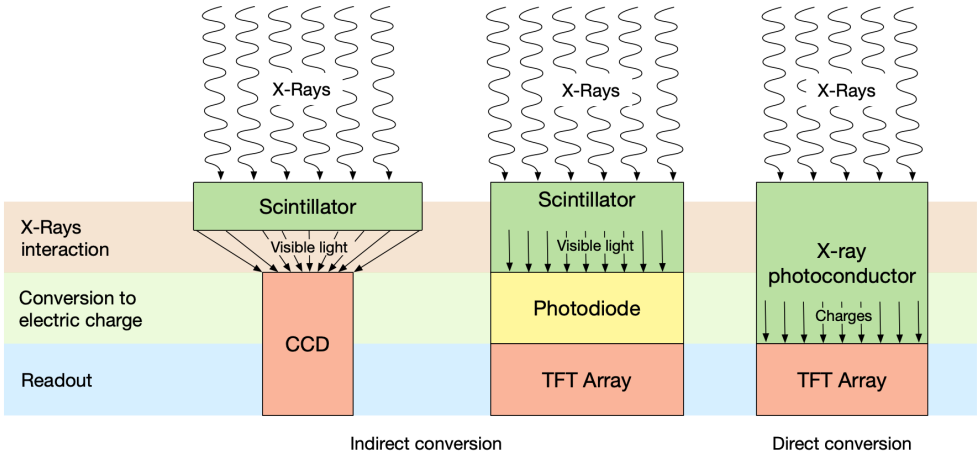

Fig. 3.3: Schema of the flat-panel structure, comparison of the direct and indirect X-ray conversion. Indirect X-ray conversion with a scintillator and CCD (left). The flat-panel with indirect conversion (middle). The flat-panel with direct conversion (right) (M. Langer, 2003), edited.

detector consists of a glass substrate. A disadvantage of indirect flat panels is a lateral diffusion of light in the scintillator that reduces sharpness and spatial resolution. To circumvent this problem, some detectors use structured scintillators - they are made from scintillation crystals of a small diameter that are perpendicular to the detector surface.

Direct conversion detectors

The top part of the direct conversion detector consists of an X-ray photoconductor layer. This layer is usually made from amorphous selenium that captures X-ray photons and converts them into electrical charge. This charge (free electron-hole pairs) is generated by the incident radiation because of the internal photoelectric effect. A bias voltage is applied to the detector so that the free charge carriers are transported to the corresponding electrodes. Their movement is almost perpendicular to both surfaces of the detector and therefore they create a minimal lateral diffusion. The collected charge is again read out by the matrix of TFTs. Thanks to the elimination of optical conversion, minimal lateral diffusion and small size of the pixels, the direct conversion detectors can offer high spatial resolution and high quantum detection efficiency (E. Kotter, 2002).

Readout mechanism

The readout mechanism is very similar for both direct and indirect detectors. Each pixel has a charge storage capacitor, an electrode for connection, and TFT switch (see figure 3.4). The pixels are arranged into a matrix - column and row detector array (Seibert and Anthony, 2006). The TFT matrix is interconnected with gates and drain lines. During the exposure, the TFT

switches are closed and the charge is collected in the storage capacitors in each pixel. After the exposure, the charges are read out, a row by row, by activating the gate line for the particular row. The local storage capacitors are connected by the TFT switches to the vertical drain lines and the charge is transported, in parallel, down the lines towards the charge amplifiers and ADCs, at the end of each column. This way the charge from each pixel is converted to the digital signal row by row and transferred to a computer.

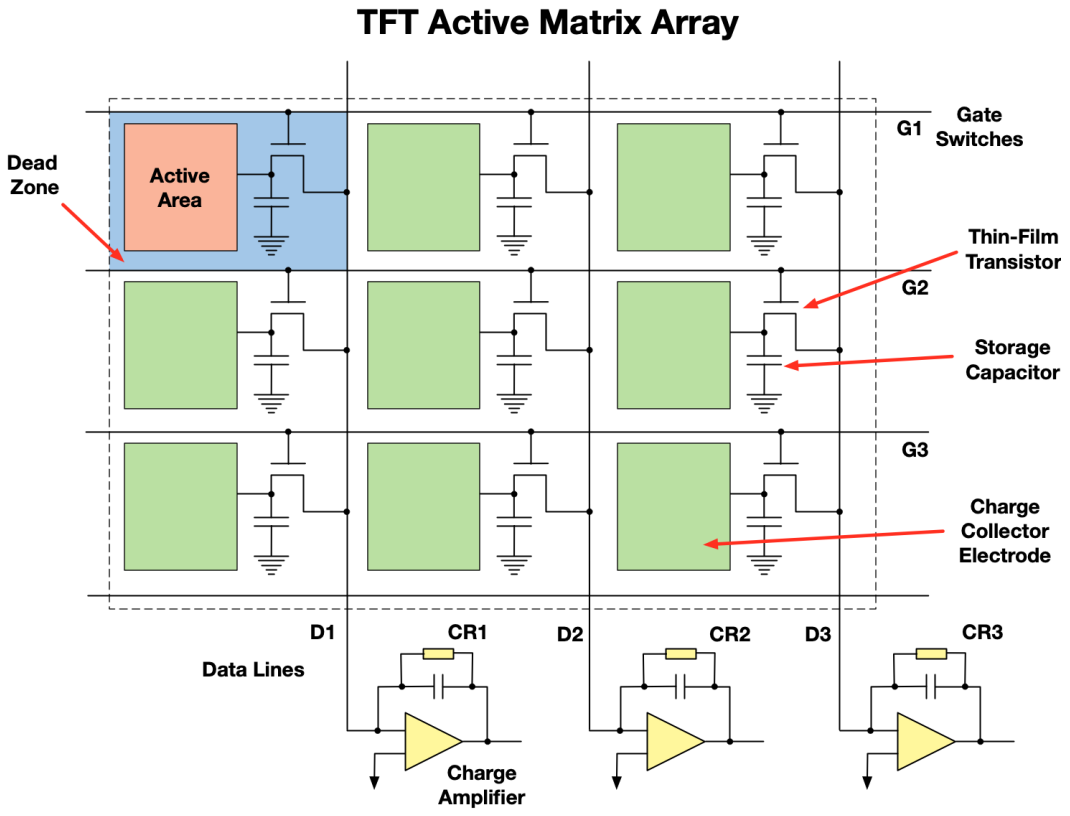

Fig. 3.4: Thin-film transistor matrix structure (Seibert, 2006), edited.

3.3 Photon Counting Detectors

All the detectors presented in the previous sections falls into the category of energy integrating detectors - they collect and sum the energy from all the incident photos. The information carried by an individual photon is lost. A high energy photon contributes more to the resulting image then a low energy once, thus reducing the contrast and enhancing the noise. The quality of the images is also decreased by the other sources of noise (dark current, electronic noise, etc.). Therefore the signal-to-noise ratio (SNR) and the dynamic range of the energy integrating detectors are limited.

The photon-counting detectors (PCDs), on the other hand, record the information from each X-ray photon individually (Russo, 2018). They represent the state of the art technology for radiation imaging. The PCDs can either simply record an incremental count of the individual

photons (simple photon counting detectors) or they can record the energy of each photon (spectroscopic detectors). In contrast to energy integrating detectors such as flat-panels, the PCDs work mostly as direct detection systems - the incident photons create electron-hole pairs in the semiconductor sensor volume which are directly collected by the detector electrodes. Thanks to this photon counting principle, most of the sources of noise, that are present in the energy integrated detectors, are eliminated and the SNR and image quality significantly improved. The other major advantage of the PCDs is the energy sensitivity - the detectors can directly measure and distinguish the energy (wavelength) of each single photon. As a result, similarly to optical sensors, a "color" image can be created. The obtained energy information is useful in many other applications and modalities such as K-edge imaging, where it can help to recognize different materials in the measured samples (Seitz and Theuwissen, 2011). There are several types of the photon counting detectors, but the most promising type is the hybrid single photon-counting detectors.

3.3.1 Hybrid Photon-Counting Detectors

The hybrid photon-counting detectors were originally designed for high energy physics (HEP) applications, especially for the collider experiments (Delpierre, 2014). The motivation was to create a detector that would be able to identify unambiguously position of events in high radiation intensity environments. Such a detector required for each pixel to have a complete electronic processing chain. The first hybrid detector was designed at CERN (Conseil Européen pour la Recherche Nucléaire) in the framework of RD19 collaboration (Heijne, 1988) (Heijne, 1994). After a successful usage of these detectors in high energy physics, other applications outside this field were explored. Medical and biological applications were ones that would benefit from state of the art features of these detectors such as full noise rejection, high speeds, detection efficiency and energy discrimination (Russo, 2018).

A single-photon counting hybrid pixel detector consists of two parts - a radiation sensor chip and a readout chip - an application-specific integrated circuit (ASIC). The figure 3.5 shows an example of a hybrid pixel detector - Timepix. The sensor chip is a semiconductor material (silicon, CdTe, etc.) that is segmented into a 2D matrix of pixels. The ASIC is segmented in the same geometry and the two chips are electrically interconnected via the bump-bonding and flip-chip techniques: a small drop (10 - 20 μm) of solder material is placed between metal pads of the pixels on both chips and they the chip are pressed together. The sensor chip has to be biased by an externally applied voltage in order to create a electric field. When a photon interacts with the sensor, an electron-hole pair is created and, because of the electric field, the charge carriers are separated and by the means of drift and diffusion move towards their respective electrodes. The resulting electric charge is collected and processed in the pixels of the ASIC. The advantage of the hybrid pixel detectors is that they allow for an individual optimization of the detector for a particular application by combining the ASIC with a sensor with optimal material (Förster et al., 2019).

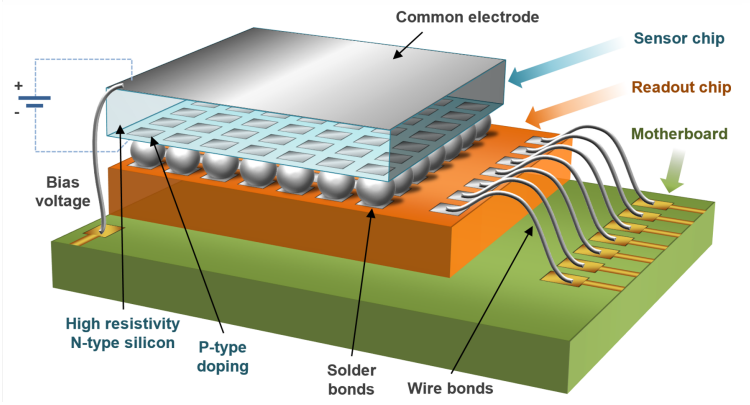

Fig. 3.5: Hybrid single-photon counting detector Timepix consisting of two parts - a sensor chip from different materials (Si, CdTe, CZT) and a readout chip interconnected together with a bump-bonding technique. (Platkevič, 2014)

Sensor materials

There are several different sensor materials that are used nowadays for the hybrid pixel detectors. The most widely used materials are silicon, cadmium telluride (CdTe), cadmium zinc telluride (CZT) and gallium arsenide (GaAs). Each material has different properties and is suitable for different applications.

Silicon is the traditional material used in semiconductors and detectors. It has relatively low mass (Z=14), great uniformity in large areas, reliability and mainly, it is relatively cheap to produce. The silicon sensors are fabricated with thicknesses between 300 μm to 1 mm and they have a reasonably good absorption efficiency in the range of 5 - 40 keV. Therefore, they are very well suitable for "soft" X-ray imagining.

CdTe and CZT are compound sensor materials with high Z. They offer better absorption efficiency for higher energies (up to approx. 250 keV). Therefore, they are used in application were high quantum efficiency is required. The commercially available thicknesses of the detectors are in the range of 1 mm to 2 mm. The thicker sensors are so far experimental (5 mm CZT (Chen et al., 2018)).

GaAs sensor is also a compound material. It offers good absorption efficiency for higher energies than silicon, but lower than CdTe. Its advantages are a low leakage current (because of its high band-gap energy), higher electron mobility and higher radiation resistance. However, there are still many challenges in the production of high quality sensors.

3.4 Medipix Detectors

Medipix detectors are a family of single-photon counting hybrid pixel detectors developed by the Medipix Collaboration (Medipix Collaboration, 2019) at CERN. The collaboration was established in 1997 between CERN, universities from Freiburg and Glasgow, and Instituto Nazionale di Fisica Nucleare (INFN) in Italy. The aim was to use the previous good experience with hybrid pixel detectors in high energy physics to explore the applications of this technology in X-ray imaging, especially in the medical field. Over the years, several generations of the Medipix chips were designed, each offering novel features. Figure 3.6 shows a photograph of the Medipix detector and its schema.

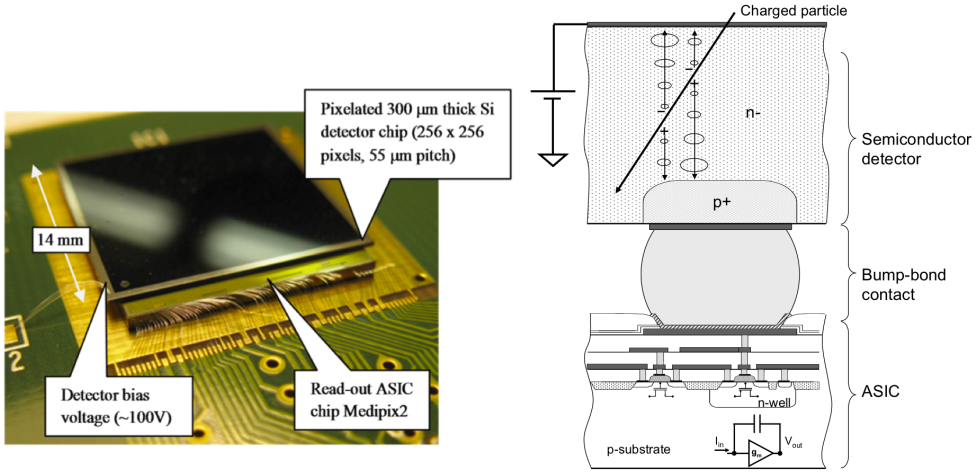

Fig. 3.6: A photograph of the Medipix2 detector with a sensor (Jakubek, 2009) and schema of the hybrid pixel detector.

The first detector designed by the collaboration was Medipx1 (Campbell and al., 1998). It was a prototype detector featuring 64 x 64 matrix of pixels with 170 μm pitch. Each pixel contained a single discriminator for energy thresholding (with 3-bit adjustment threshold) and 15-bit shift register behaving as a counter. The first chip, bump-bonded with GaAs sensor, was successfully tested for the use in medical and biological applications with several proof of concept measurements. Following the Medipix1 success, the collaboration designed several successor chips, each improving over the previous one.

3.4.1 Medipix2 Detector

The Medipix2 detector (Llopart et al., 2001) was a first Medipix detector used widely in the scientific community, and even commercially, for X-ray imaging. Thanks to the advances in Complementary Metal-Oxide Semiconductor (CMOS) technology, it was possible to integrate more advanced processing electronics in each pixel and at the same time reduce the pixel size. The Medipix2 readout chip is fabricated in IBM 0.25 μm technology and is organized as matrix of 256 x 256 pixels with 55 μm pitch. The chip has dimension of 16 x 14 mm and is divided

into an active area at the top (1.982 cm^2) and non-sensitive periphery area at the bottom. (see figure 3.7). The periphery contains 117 wire-bonding pads, biasing DACs and control logic and is placed at the bottom, to minimize the dead area in the other three edges of the chip. The digital part of the pixel matrix is organized in such a way that the pseudo-random counters of each pixel in a column are interconnected, creating a matrix of 256 x 3584-bit shift registers. These registers are connected to the 256-bit fast shift register (FSR) in the periphery. This FSR is used for reading (shifting-out) of the data or writing of the pixel adjustment bits. It is also used for setting of the values of the 13 periphery DACs and reading of the chip identification code.

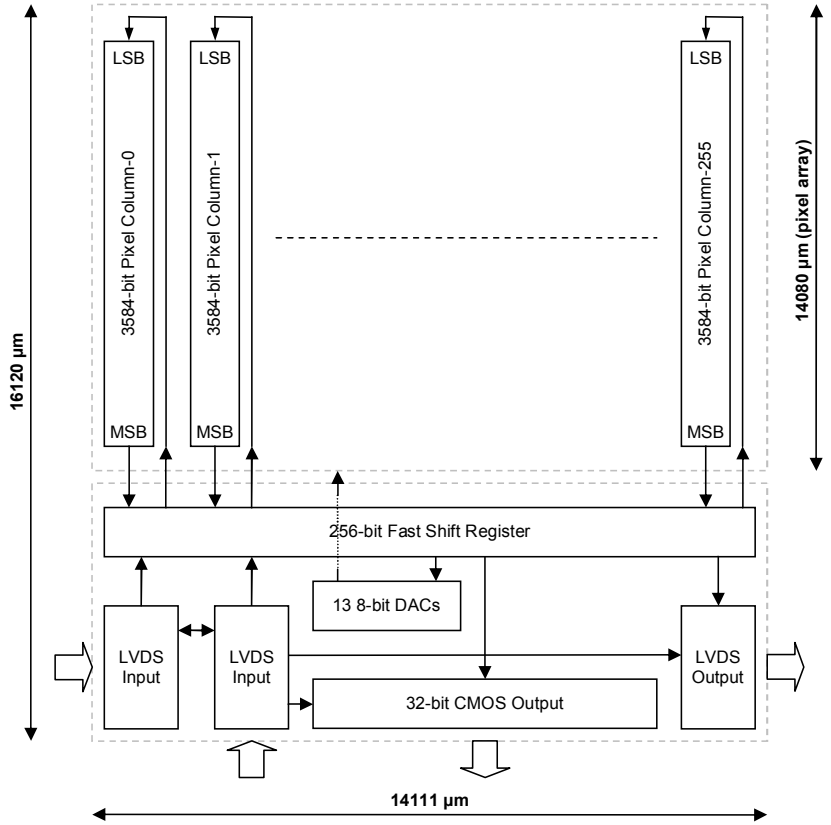

Fig. 3.7: Medipix2 surface plan and the block diagram (Vykydal, 2004).

Each pixel of the Medipix2 chip is divided into a digital and an analog part (see figure 3.8). The analog part contains a small feedback capacitance, charge sensitive preamplifier (CSA), test capacitance and two discriminators (adjustable by 3 bit threshold) that form an acceptance energy window. The digital part contains double discriminator logic, 13 bit shift register (used as pseudo-random counter) and CMOS logic for counter, data shifting and 8-bit configuration storage (Llopart et al., 2001).

The pixel can work in two modes of operation, depending on the chip's shutter signal. When the shutter signal is not active, the pixel's 13-bit register act as a shift register and the acquired data is shifted-out. In the case the shutter signal is active, the chip and the pixels work in

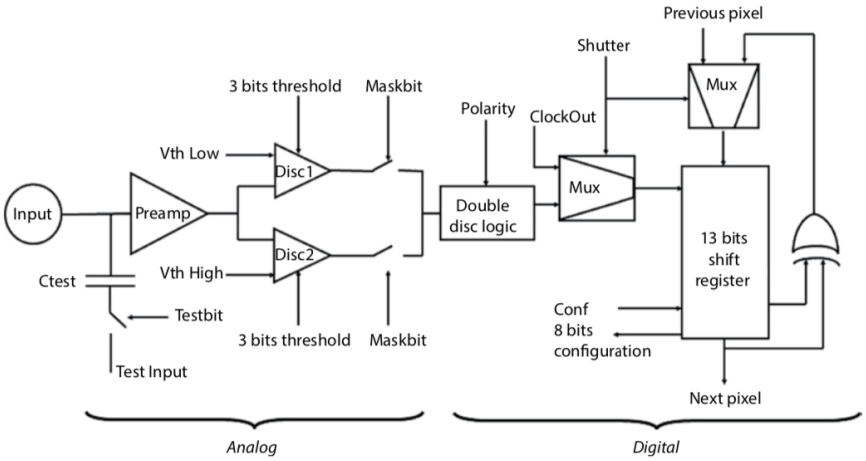

Fig. 3.8: Schema of the Medipix2 pixel (Llopart et al., 2001).

the acquisition mode and the 13-bit register acts as a pseudo random counter. The charge generated in the sensor by an incident photon is collected in a small feedback capacitance and amplified by a CSA. Then, the output pulse from CSA is compared with the two discriminators, and if it is accepted, the counter is incremented.

The Medipix2 chip was designed in the way, that the front-end electronics is able to collect either holes or electrons, based on the type of the used sensor. The chip has minimal reported threshold of 1000 e, can be readout with a frequency of 200 MHz and has a power consumption of about 500 mW.

3.4.2 Timepix Detector

The Timepix chip (Llopart et al., 2007) is a successor to the Medipix2 chip, introduced in 2006. It brings the possibility to measure time of arrival and perform direct spectroscopic measurements. The chip has the same dimensions, number of pixels and read-out architecture as Medipix2. Each pixel has charge sensitive preamplifier, single discriminator with 4 adjustment bits and 14-bit pseudo random counter. The pixel can work in three different modes (see figure 3.9):

- **Counting (Medipix) mode** - same as Medipix2 chip, each incident event above the threshold increments the counter.

- **Time over Threshold (ToT) mode** - the counter works as Wilkinson-type analog-to-digital converter (ADC). The counter is incremented continuously on every clock as long as the signal is above the threshold. The length of the pulse from the charge amplifier and discriminator is directly proportional to the input charge (energy). Therefore, the number of measured clock pulses is proportional to the deposited charge in the sensor.

As a result, the energy of the incident photons can be obtained from ToT counts by using the per pixel calibration method (Jakubek, 2011).

- **Time-of-Arrival (ToA)** - the counter works as a timer and measures the arrival time of the event. The counter is incremented continuously on every clock since the arrival of the event until the shutter is closed. The maximum possible time with a 10 MHz clock is about 1 ms.

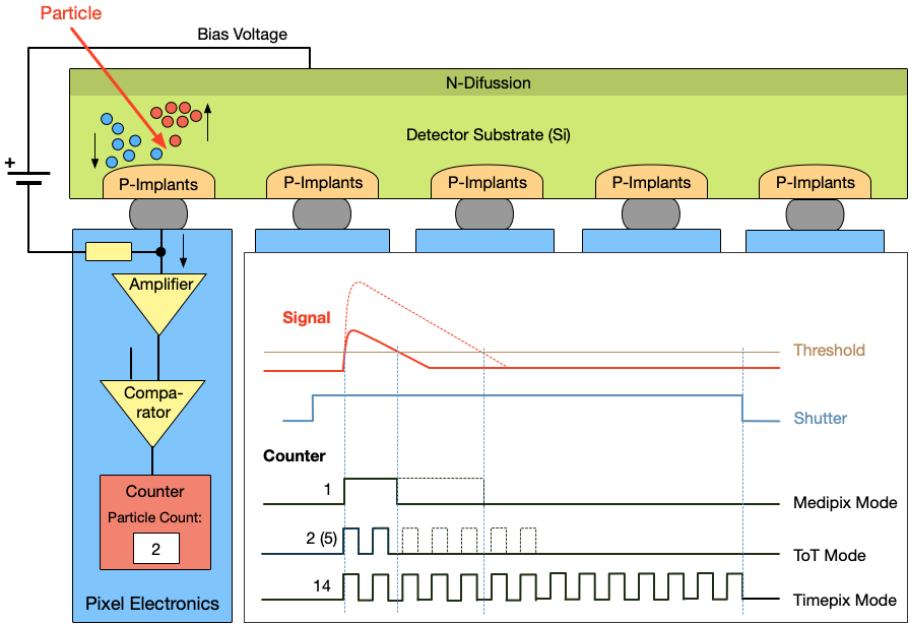

Fig. 3.9: Schema of the principle of signal acquisition of the Timepix detector

Introduction of the Timepix chip has opened wide range of new applications outside of the X-ray imaging field. Thanks to the ToA and ToT measurements, the chip can be used in high energy physics as a particle tracker, in space as a dosimetric device (Turecek et al., 2011), as a neutron detector (Uher and Jakubek, 2011), for phase contrast imaging (Jakubek and Kroupa, 2011), XRF imaging (Zemlicka et al., 2009), and many other applications.

3.4.3 Medipix3 Detector

Medipix3 chip(Ballabriga et al., 2011) (see figure 3.10) is a successor to Medipix2 chip fabricated in 0.13 μm technology introduced in 2007. Similarly as it predecessor, it creates images by counting in each pixel the number of particles that hit that particular pixel. However, it comes with many improvements and new features over Medipix2: possibility of color imaging, dead time free operation and charge summing mode. The chip has the same pixel matrix size of 256 x 256 pixels with 55 μm as Medipix2. Each pixel contains two 12-bit pseudo random counters, two discriminator adjustable with 4 bit threshold, charge sensitive amplifier and digital logic for read-out, charge summing arbitration and different modes of operation. The

pixel counter's depth can be configured to work in 1-bit, 6-bit, 12-bit and 24-bit mode. The 24-bit mode is achieved by chaining two 12-bit counters together.

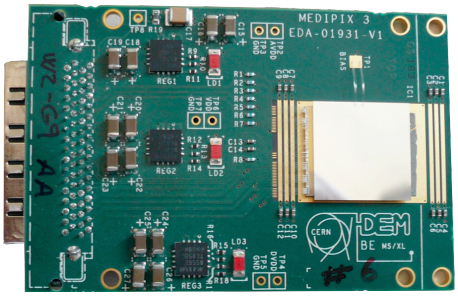

Fig. 3.10: A photo of the Medipix3 chip wire-bonded on a chip board PCB.

The Medipix3 chip can be configured to operate in *fine pitch mode* where each pixel is bump-bonded to the sensor or in *spectroscopic mode* where only one pixel in a group of four pixels is bump-bonded, effectively increasing pixel pitch to 110 μm and offering up to eight threshold and counters. The spectroscopic mode improves the energy selection and allows for images with up to 8 "colors". Furthermore, the chip front-end can be programmed in two different gain modes: *high gain mode* that reduces the noise, but also reduces the linearity and maximum count rate and the *Low gain mode* that has higher noise, but improves the linearity and dead time.

The Medipix3 chip can be programmed in these operation modes:

- **Single pixel mode** - each pixel counts independently, similar to counting mode of Medipix2 or Timepix detector.
- **Charge summing mode** - charge summing circuits and arbitration logic mitigate the effects of charge sharing between pixels. The charges are summed in every 2x2 pixel clusters and the total charge is assigned locally to the pixel with the highest charge.
- **Spectroscopic (color) mode** - the pixels are grouped into clusters of 2x2 pixels, where only one pixel is bump-bonded to the sensor. The effective pixel pitch is 110 μm and resolution is decreased to 128 x 128 pixels. However, each 110 μm pixel can use up to 8 thresholds. The spectroscopic mode can be used together with charge summing mode. In that case, the charge summing arbitration is performed in the total area of 220 x 220 μm.

3.4.4 Timepix3 Detector

The Timepix chip was originally designed to be a timing measurement chip with possibility of measuring also the timer-over-threshold (ToT). The ToT functionality has proven to be useful in many applications and was the most widely used operation mode of the Timepix

detector. However, there are also many applications that would benefit of simultaneous usage of ToA and ToT modes, which Timepix does not support. Timepix3 chip (see figure 3.11) was developed as a successor of Timepix to extend and improve its functionality. The main driving requirements were: simultaneous ToA and ToA measurement, minimal dead time, monotonic ToT measurement in both detector polarities (holes and electrons) and improved time resolution.

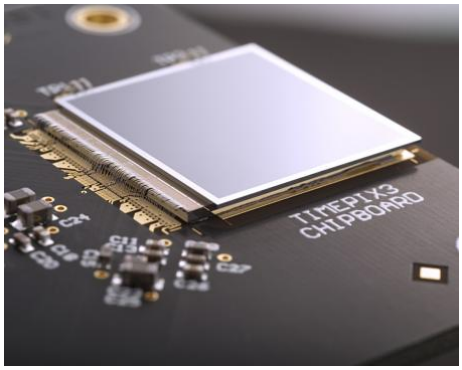

Fig. 3.11: A photo of the Timepix3 chip (Medipix Collaboration, 2019)

Timepix3 (Poikela et al., 2014) is fabricated in 130 nm CMOS technology and has dimensions of 14.1 x 16.2 mm. It allows simultaneous ToA and ToT measurements and improves the time resolution of Timepix by factor 6. It has zero-suppression readout (only hit pixels are read-out) and is capable of detecting particle rates of about 40 Mhits/cm^2/s. Table 3.1 shows comparison between Timepix and Timepix3 chips.

Parameter	**Timepix (2006)**	**Timeix3 (2013)**
Pixel arrangement	256 x 256	256 x 256
Pixel size 55 x 55 μm	55 x 55 μm	55 x 55 μm
Technology	250 nm CMOS	130 nm CSMO
Acquisition modes	1. Charge (iToT) 2. Time (ToA) 3. Event Counting	1. Time (ToA) and Charge (ToT) 2. Time (ToA) 3. Event Counting and iToT
Readout type	Full Frame	Data Driven Frames
Zero suppression readout	NO	YES
Dead time per pixel	> 300 μs	> 475 ns
Minimum timing resolution	10 ns	1.562 ns
Minimum detectable charge	750 e-	500 e-
Output bandwidth	1 LVDS < 200 Mbps 32 CMOS < 3.2 Gbps	1 to 8 LVDS @ 640 Mbps < 5.2 Gbps

Tab. 3.1: Timepix and Timepix3 parameters comparison.

Data Readout

One of the main new features of Timepix3 chip is the novel readout architecture. The data from the pixel matrix can be either read-out whole as a frame, or the chip can be configured to work in a zero suppression mode - data driven mode. In this mode only pixels that are hit are read-out. Moreover, when the pixel is hit, it sends its data (a packet) immediately and its ready to accept another hit. This reduces significantly the dead time. The pixel data packet are sent from the pixel matrix to periphery where they are read-out by up to 8 high speed serial scalable low-voltage signaling (SLVS) links. The data on each link is encoded in 8b/10b encoding. The advantage of this encoding is that the output data stream can be used for clock and data recovery (CDR), thus not requiring separate clock signal. Each link can support read-out frequencies from 40 MHz to 320 MHz at double data rate (DDR), achieving total maximum output bandwidth of 5.12 Gb/s. The packet-based (date driven) readout is advantageous especially for matrix occupancies under 50 % (see figure 3.12). Moreover, the packet-based readout has also an advantage that it is continuous, thus the duty cycle of the chip is 100 % as long as the total particle rate is not higher than 40 Mhits/cm^2/s.

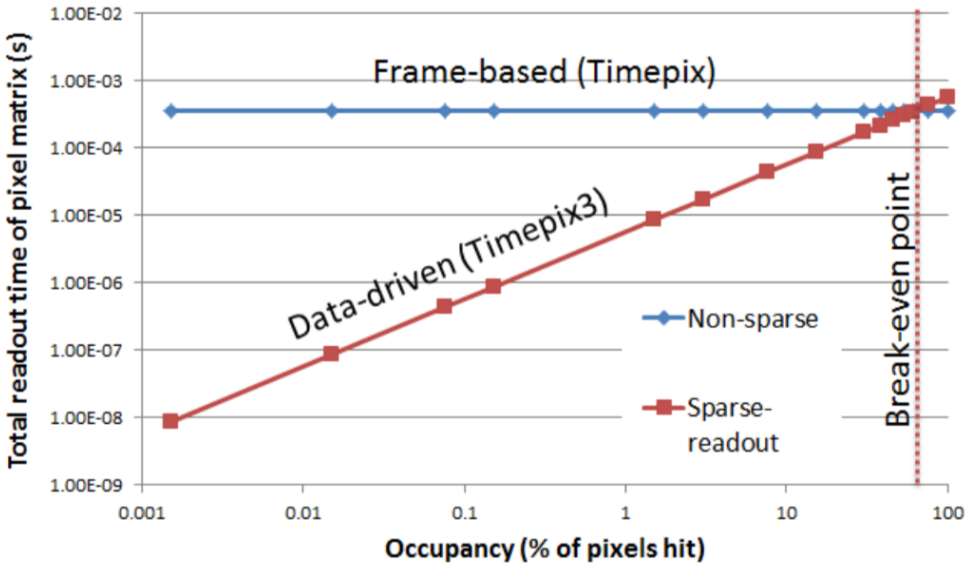

Fig. 3.12: Readout times of a pixel matrix with a frame-based (non-sparse) and a packet-based (sparse) readouts (Poikela et al., 2014).

Pixel matrix

The pixel matrix of Timepix3 has the same dimensions as previous chips - 256 x 256 pixels with 55 μm pitch, but contains much more processing logic. Also, every group of 4x4 pixels forms a a super pixel that contains more logic which is shared among these pixels. Figure 3.13 shows a schema of the pixel and super pixel. The analog part contains charge sensitive preamplifier with leakage current compensation, local adjustable threshold (4-bits) and discriminator. The digital

part contains synchronization logic to synchronize asynchronous hits to the on-pixel clock, 14-bit time stamp register, a 10-bit linear-feedback shift register (LSFR) for ToT measurement and configuration logic. (Poikela et al., 2014) The super pixel contains a voltage-controller oscillator (VCO) that generates high frequency clock (640 MHz) for the precise time measurements in each pixel in the group.

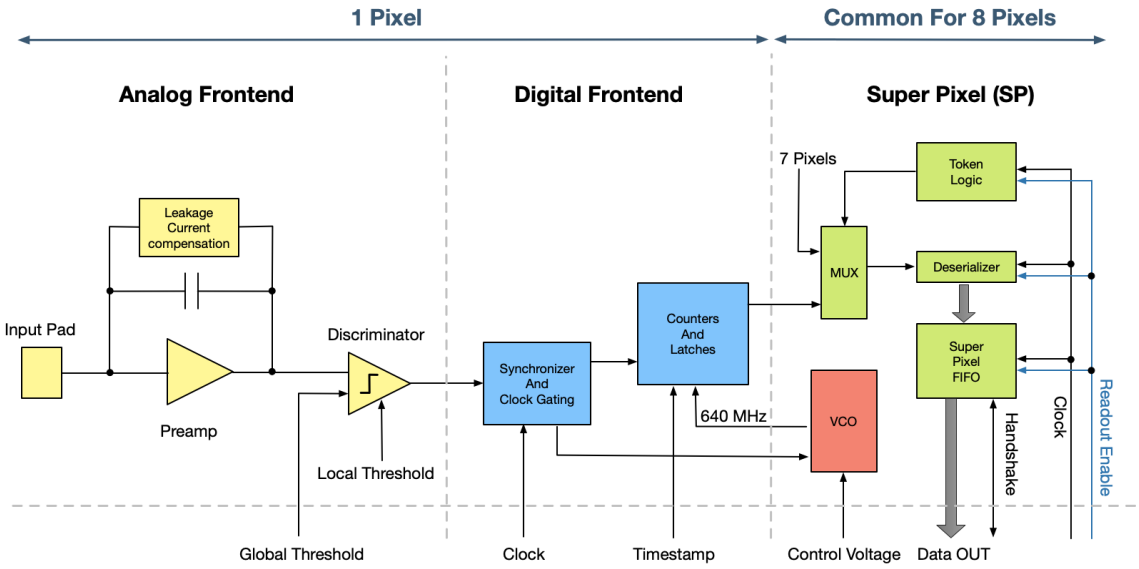

Fig. 3.13: Schema of Timepix3 pixel.

Principle of operation

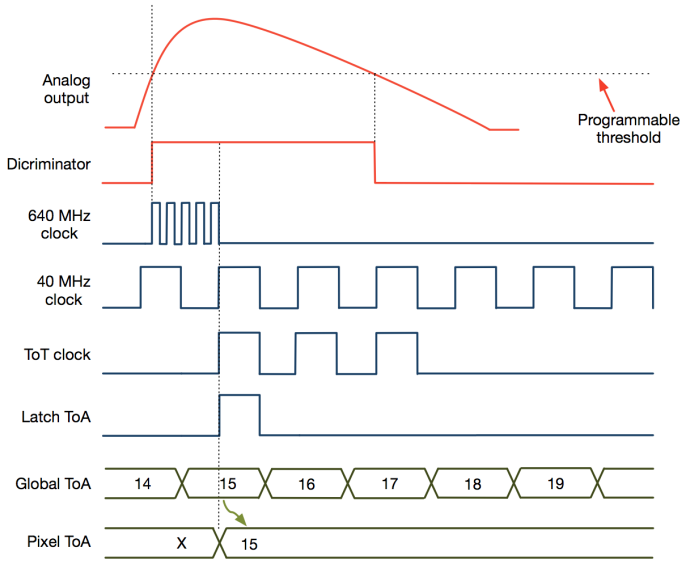

Fig. 3.14: Operation principle of Timepix3 pixel

When the pixel is hit by an particle its charge is collected in the analog part of the pixel, compared with the selected threshold and, if the charge is above the threshold, it is processed

by the digital part. The 640 MHz clock is started on the rising edge of the discriminator output pulse and is running until the first rising edge of the global 40 MHz clock. This way the high precision timestamp (Fast ToA) is measured. At the same time, the coarse time stamp (ToA) is registered into the 14-bit time counter and the ToT measurement is started (see figure 3.14). The ToT measurement is stopped when the analog output from the amplifier sinks under the selected threshold. At this moment, a pixel data packet is generated. Then, depending on the configured measurement mode, the packet is send to the periphery immediately, in the case of the data driven mode, or is kept in the pixel until it is readout, in the frame mode.

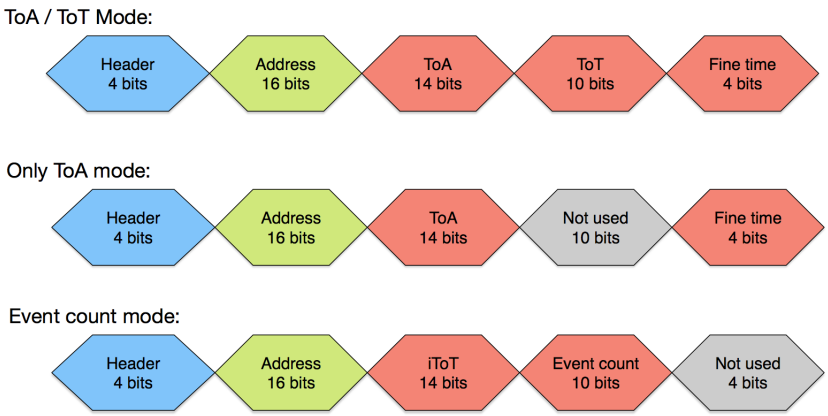

Fig. 3.15: Timepix3 pixel data packets

The data packet is always 48 bit long and contains a header, pixel address and data payload. The Timepix3 can be configured to work in three different acquisition modes that influence the content of the pixel packets (see figure 3.15):

- ToA / ToT mode - the pixel measures both ToA and ToA simultaneously with time precision of 1.56 ns. The ToA timestamp is 14-bit long and ToT values 10-bit long.
- Only ToA mode - the pixel measures only ToA information
- Event counting mode - the pixel measures integral ToT information and number of particles that hit the pixel. The iToT values are 14-bit long and event count values 10-bit long.

4 Results

This chapter describes the gradual research work done in characterizing the hybrid single photon counting pixel detector Timepix3 and exploring its potential usage in different imaging modalities. The motivation was to fully exploit all the advanced functionality and features of this detector. As a first step, it was necessary to create the needed infrastructure, DAQ hardware and software, to operate the Timepix3 chip. Energy calibration and time correction methods were developed in order to obtain valid data with physics meaning (ToT counts converted to energy, ToA values to time). Then the different Timepix3 modalities were explored:

- **Counting**. This modality was evaluated in the radiography applications. A very fast radiographic measurement was performed and the resulting images have demonstrated advantages of usage of Timepix3: high resolution and high frame rates.

- **Energy**. New method was developed to suppress the unwanted signals from intrinsic effects of the CdTe sensors. The energy information was then used for energy filtering and the detector was evaluated in the SPECT imaging application.

- **Time of arrival**. The time modality of the detector was explored in PET application. The time information was used to find coincidence gamma events from positron annihilation.

- **Time and energy**. The time and energy information together were explored in the multi-layer Compton camera application, where the both information were used to recognize the Compton scattering events and to reconstruct the location of the gamma source.

- **Precise time and energy**. The Compton camera concept was further improved by fully exploiting the fine time resolution of Timepix3. Thanks to the precise time it was possible to measure the charge collection time in sensors and thus to measure the depth of the interaction in the sensor. This permitted us to create a monolithic single layer Timepix3 Compton camera.

These results were successively published in scientific journals and this chapter presents them in a form of summaries and discussions to these publications:

- **Publication A: Turecek D.**, Jakubek J., Soukup P., "*USB 3.0 readout and time-walk correction method for Timepix3 detector*", JINST Vol 11, C12065, December 2016

- **Publication B:** Trojanova,E. Jakubek, J. **Turecek, D.** Sykora, V. Francova, P. Kolarova V. and Sefc, L. "*Evaluation of Timepix3 based CdTe photon counting detector for fully spectroscopic small animal SPECT imaging*." JINST, Volume 13, Issue 1, 2 January 2018

- **Publication C: Turecek D.**, Jakubek J., Trojanova E., Sefc L., Kolarova V., "*Application of Timepix3 based CdTe spectral sensitive photon counting detector for PET imaging*"., Nuclear Instruments & Methods In Physics Research Section A, Volume 895, p84-89 (2018)

- **Publication D: Turecek D.**, Jakubek J., Trojanova E., Sefc L., "*Compton camera based on Timepix3 technology*", JINST Vol 13, C11022 (2018)

- **Publication E**: **Turecek D.**, Jakubek J., Trojanova E., Sefc L., "*Single Layer Timepix3 Compton Camera*". Prepared for publication.

4.1 Publication A - USB 3.0 readout and time-walk correction method for Timepix3 detector

This first publication have laid out the ground work for the following research. When the Timepix3 readout chip was designed at CERN, with its advanced features, it was clear that this chip can make a significant impact in many applications, including preclinical medical imaging. Therefore, from the all single photon counting detectors, Timepix3 was selected as a good candidate detector for exploring the new methods and algorithms in multi-modal imaging. However, in order to exploit all the features of the detector, it was necessary to create a hardware and software infrastructure. The first publication describes the results of the development of a new readout device for Timepix3, the DAQ software and Timepix3 optimization and calibration methods.

4.1.1 AdvaDAQ Readout Hardware

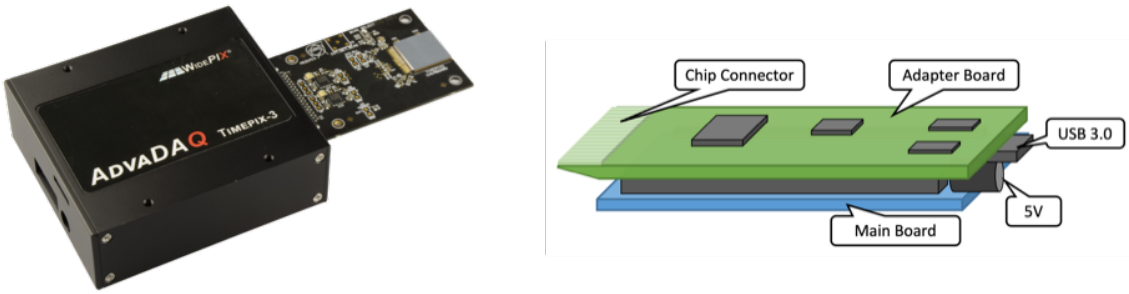

Fig. 4.1: A Photo of the AdvaDAQ readout interface (left). Schema of the AdvaDAQ readout (right).

The aim in designing the new readout interface for Timepix3 chip was to exploit all of its features. Since the Timepix3 is capable of transferring 5 Gbps, it was decided to design the readout interface with USB 3.0 connectivity, that allows high transfer speeds and high flexibility. The interface was named AdvaDAQ and consists of two board - the general USB 3.0 main board with a FPGA and an adapter board with electronics for Timepix3 detector (see figure 4.1).

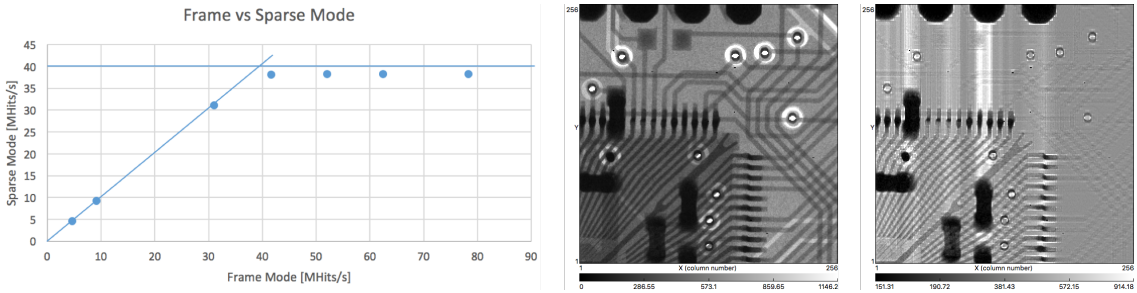

Fig. 4.2: Performance of the AdvaDAQ readout

The performance of the AdvaDAQ readout was tested in several tests. One of the test was to evaluate maximum throughput of the interface in the data driven mode (see figure 4.2). A

sample (PCB board) was positioned in front of the detector and was irradiated with X-rays. The intensity of the X-rays was gradually increased and the data was taken in both frame based and data driven mode. From the measurements it was determined that Timepix3 connected to AdvaDAQ readout is capable of acquiring 40 Mhits/s/cm^2. This is more than sufficient for most of the applications, including spectroscopic radiographies.

4.1.2 DAQ Software Pixet

In order to operate Timepix3 detector it was not only necessary to create the readout interface hardware and its firmware, but also develop a software that would be able to control the interface, acquire the data, transfer them to PC, visualize, process and analyze them. The DAQ software package Pixet was developed (see figure 4.3). The software permits users to control all the functionality of the detectors and readout interfaces. It supports not only Timepix3 detectors, but also other detectors from Medipix family (Medipix2, Timepix, Timepix2) and other readout interfaces (MiniPIX, MiniPIX TPX3, AdvaPIX, WidePIX, etc.).

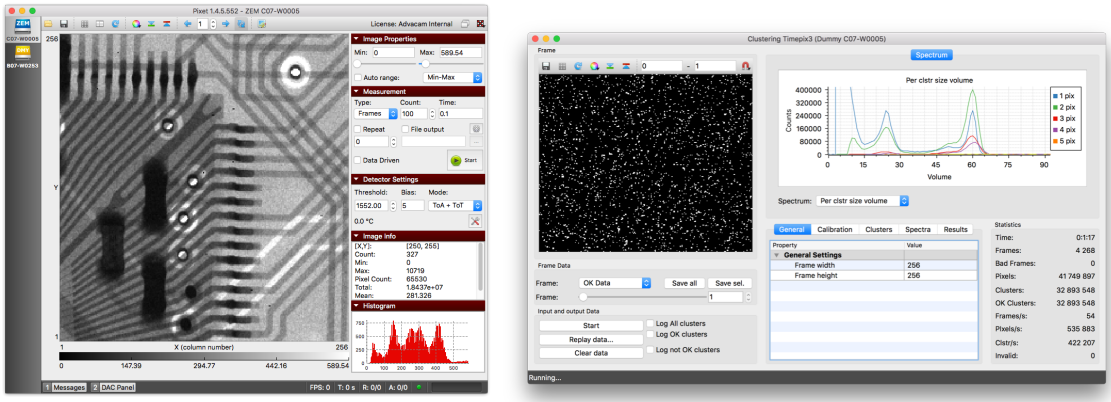

Fig. 4.3: Screenshots of the Pixet software

The software allows user to acquire and see the measured data. It features a very flexible architecture and can be easily extended with add-on modules - plugins for data processing and visualization, and hardware libraries for interfacing with different hardwares (detectors, X-ray tubes, motors, etc.). Furthermore, dedicated algorithms for Timepix3 detector were developed - calibration and correction procedures and cluster recognition algorithm.

4.1.3 Timepix3 calibration methods and first measurements

Timepix3 chip can measure Time-over-Threshold (ToT) and Time-of-Arrival (ToA) at the same time. The measured ToT values has to be converted from raw values into energy in keV. Since the Timepix3 measures the ToT similarly as Timepix chip, a slightly modified per-pixel energy calibration method was developed for Timepix3 and tested with radiation sources.

Timepix3 can measure ToA very precisely with resolution of 1.56 ns. However, the ToA values are dependent on the energy of the incident particle. This effect is called Time-walk and is caused by different slope and amplitude of the signals generated by the particle in the pixel circuitry. This effect can be corrected by calibrating the energy-time dependence. A new correction method was developed that uses a radiation source to calibrate this dependence. This method improves significantly the time precision of the measured data. The method was verified with a measurement of cosmic muons (see figure 4.4).

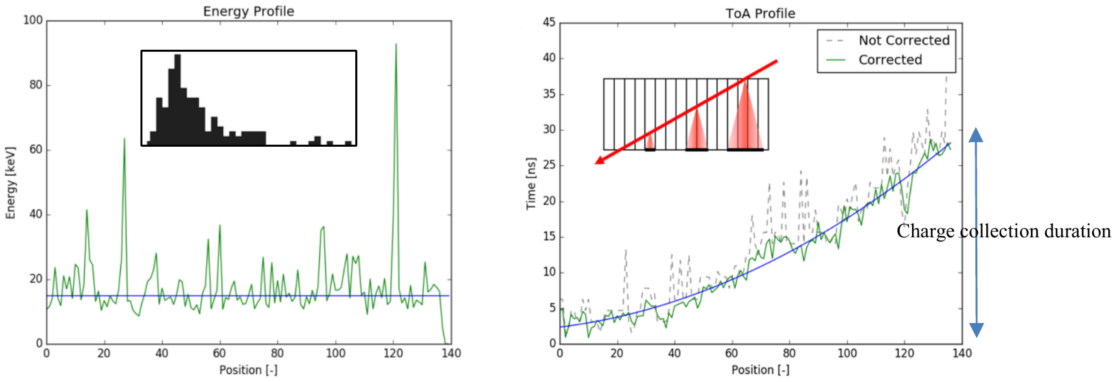

Fig. 4.4: Time-walk correction: Muon track energy profile with energy distribution (left). Comparison of corrected and not corrected time profile (right).

When all the basic infrastructure and correction methods were developed, the new hardware and software for Timepix3 were tested with several measurements. Because of the fast data acquisition of AdvaDAQ readout and energy information in each pixel thanks to Timepix3, it was possible to make a very fast full spectroscopic radiography. Figure 4.5 shows an example of a radiography of a PCB sample. The measured data was divided into multiple energy bins and each bin was assigned a color, thus creating a "color" X-ray radiography. Each color in the image corresponds to a different material.

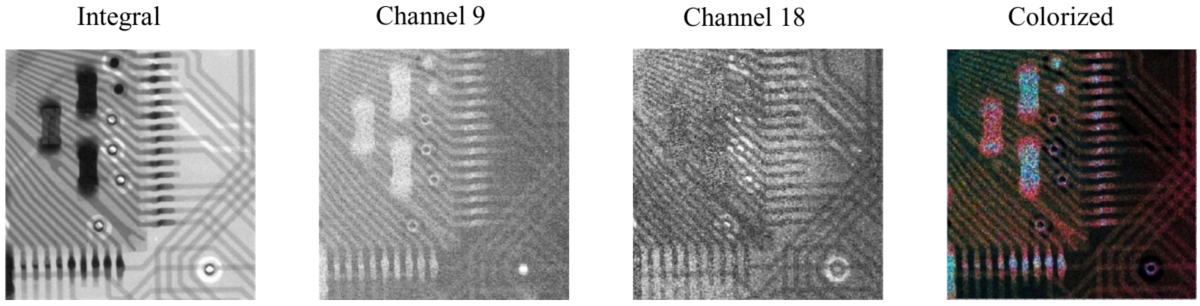

Fig. 4.5: Fast spectral X-ray radiography at hit-rate 30 Mhits/s: the integral image is shown left. Two energy bins normalized by integral image are shown in the middle. The color interpretation is shown on the right side.

4.1.4 Discussion

The work described in this publication prepared all the necessary infrastructure for Timepix3 detector in order to explore new imaging methods and modalities. The hardware, software, calibration and correction procedures were verified. A very fast full spectroscopic radiography measurement was performed that demonstrated the advanced features of Timepix3 detector in imaging applications. In the future the "color" X-ray radiographies can be extended in to full "color" X-ray CT.

My contribution in the first publication was writing the text, taking part in design of the AdvaDAQ readout hardware, programming of the firmware for the FPGA, developing all the software and algorithms and performing the first tests and measurements.

4.2 Publication B - Evaluation of Timepix3 based CdTe photon counting detector for fully spectroscopic small animal SPECT imaging

The aim of the second study was to evaluate Timepix3 detector properties in single photon emission tomography (SPECT) measurements. The AdvaDAQ readout interface was improved so that the Timepix3 chip is mounted on the metal support for better heat dissipation and directly connected to the PCB for better electrical signals. Also, support for high negative bias voltage (up to -500 V) was developed to support thick CdTe sensors. This improved interface was named AdvaPIX TPX3 (see figure 4.6).

Fig. 4.6: AdvaPIX TPX3 readout interface

4.2.1 Energy Spectra Reconstruction

One of the great advantages of Timepix3 is that it can very precisely measure the energy of the incident photons. This energy information can be used to improve the measured images by filtering out the unwanted data by its energy. However, there are several unwanted effects intrinsic to CdTe sensors that are affecting the quality of the measured data. First effect is the internal X-ray fluorescence of CdTe sensor. When the photon with a higher energy hits the sensor, the photoeffect can in some cases result in Kα excitation of the sensor atoms Cd or Te followed by emission of characteristic X-ray photon with an energy of 25 keV. The secondary event is usually detected as a distinct event within several nanoseconds. The second effect is the Compton scattering of the primary gamma in the sensor that also results in two coincidence events. Thanks to Timepix3 high precision time measurement, these two events can be detected. A special spectrum reconstruction algorithm was developed that finds such events, determines the primary event and combines the secondary event back to the original one. The algorithm works very well and improves the energy spectrum significantly. The figure 4.7 shows the energy spectrum before and after application of this algorithm.

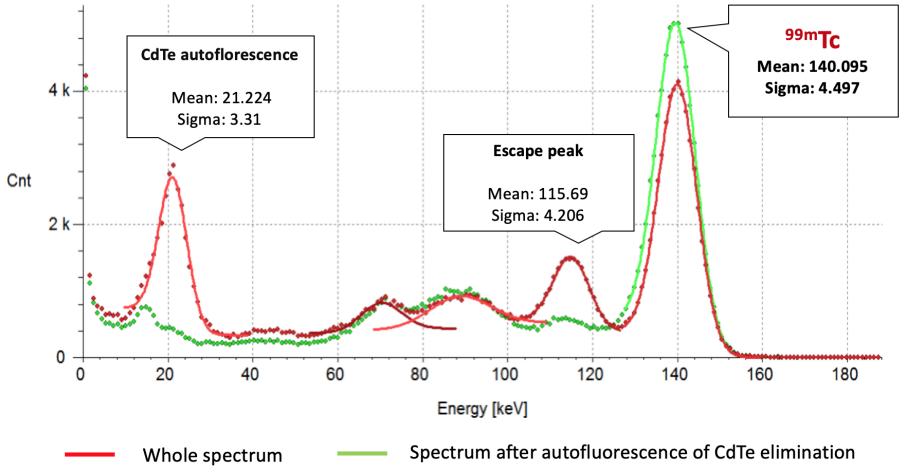

Fig. 4.7: Energy spectrum before and after correction of auto-fluorescence of CdTe.

4.2.2 Experimental Setup and Measurements

AdvaPIX TPX3 device with 1 mm thick CdTe sensor was chosen for the experiments to ensure good detection efficiency for higher energies (140 keV). The device was shielded by lead and equipped with a collimator with double-cone shaped pinhole of 500 μm in diameter. The detector was placed in the distance of 10 cm from the the two measured samples (see figure 4.8). First measurement was performed with a cylindrical PMMA phantom (45 mm in diameter) with drilled cavities to simulate the body of a rodent. The cavities were filled with a solution of water and radioisotope ^{99m}Tc. The second measurement was performed with a real sample for preclinical imaging - a living mouse under anesthesia injected with ^{99m}Tc solution.

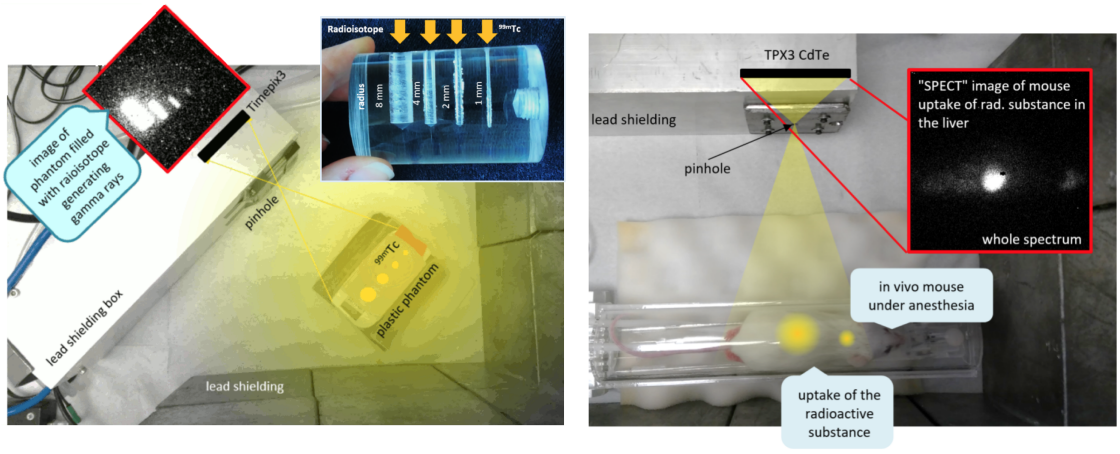

Fig. 4.8: SPECT measurement experimental setup

4.2.3 Results

The data was taken for both samples in Timepix3 event-by-event mode, recording for each photon its time information and deposited energy. The energy spectrum correction was applied and images generated. Images for the full energy range are shown in figure 4.9 and 4.10 left. The phantom cavities and the normal biodistribution of ^{99m}Tc in stomach, thyroid gland, salivary glands and bladder in the mouse are clearly visible in the images.

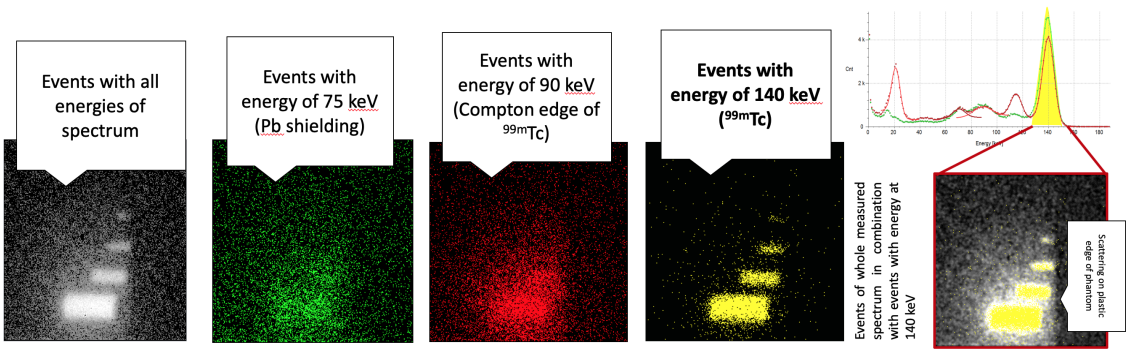

Fig. 4.9: Phantom sample. Full energy spectrum image (left), images for different energy bins (right).

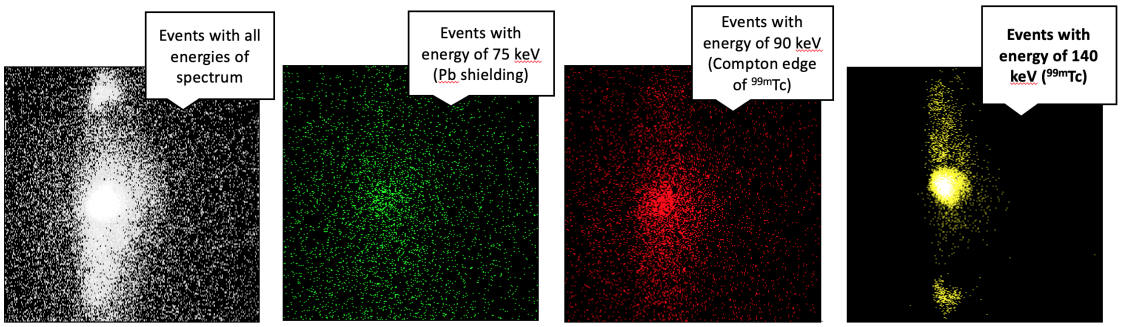

Fig. 4.10: Mouse. Full energy spectrum image (left). Images for different energy bins (right).

Thanks to the energy information, a sequence of images from events with a specific energy interval could be generated (see figure 4.9 and 4.10 right). Each energy interval enhances different part of the spectrum (Pb shielding, Compton edge, etc.). By selecting the proper energy window (125 - 150 keV), the background signal can be reduced and the image contrast improved.

In order to quantify the image quality improvement before and after filtering, the signal to background ratio (SBR) was used. The SBR is calculated as ratio between average signal in the image area with the presence of ^{99m}Tc (signal) to the image area with zero density of the ^{99m}Tc (background signal). Table 4.1 shows a SBR analysis for both samples and 3 different background areas (see figure 4.11) from closest area with the signal (P1) to most distant one (P3). It is visible that the application of the spectrum correction and filtering by the energy interval can improve the image quality by factor of 7 in the case of phantom and by factor of 8 in the case of the mouse. Moreover, the spatial resolution is also improved.

Spectrum filtering steps	Phantom			Mouse		
	P1	P2	P3	P1	P2	P3
Uncorrected spectrum	16.8	70.4	77.9	125.8	60.8	99.3
Energy window (135-150 keV)	103.9	467.6	467.6	453.4	453.3	1020.3
CdTe XRF correction	17.3	69.0	78.3	121.2	59.26	106.67
All corrections applied	101.3	582.6	517.9	450.6	579.3	1013.7
SBR improvements	6	8	7	4	10	10
		7x			8x	

Tab. 4.1: SBR analysis for PMMA phantom and in-vivo mouse measurement. Table summaries SBR improvements with different applied spectrum filtering.

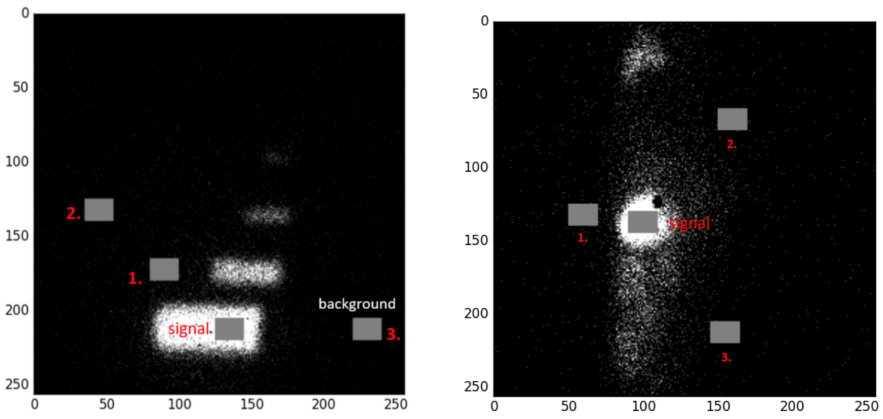

Fig. 4.11: Selected image areas for SBR analysis for PMMA phantom (left) and in-vivo mouse measurement (right).

4.2.4 Discussion

It was demonstrated in this publication that Timepix3 detector in combination with thick CdTe sensor and collimator can be used for SPECT measurements. Timepix3 also offers a superior energy and spatial resolution compared to the conventional scintillator based cameras. Moreover, thanks to the precise time and energy measurement the unwanted signal caused by XRF and Compton scattering in the sensors can be suppressed and thus the image quality significantly improved. Even though the measurements in this publication were performed only in 2D, they can be easily extended into full 3D SPECT measurement by creating a ring detector composed of multiple Timepix3 units. Moreover, thanks to the small size of the AdvaPIX readout, it is possible to create a small and portable SPECT detector. This is advantageous, because the detector can be easily transported to the laboratory (e.g. with animals) and the imaging can be made in place.

My contribution in this publication was helping with the technical side of the measurements and developing of the XRF and Compton scattering suppression algorithms.

4.3 Publication C - Application of Timepix3 based CdTe spectral sensitive photon counting detector for PET Imaging

The Positron emission tomography (PET) is a nuclear medicine functional technique used in oncology and preclinical studies on small animals. The conventional PET systems are using scintillator based cameras with spatial resolution in order of 1 mm and energy resolution of about 10 - 20 %. Timepix3 detector can offer smaller pixel size (55 μm) and better energy resolution. The goal of this publication is to make an initial study to evaluate Timepix3 applicability in the PET imaging.

4.3.1 Experimental Setup and Measurement

For the PET measurement two AdvaDAQ readouts with Timepix3 detectors equipped with 2 mm thick CdTe sensors were chosen. The AdvaDAQs were connected to a special FPGA board that provided common clock for both Timepix3 chips in order to have fully synchronous measurement of ToA (see figure 4.12 a).

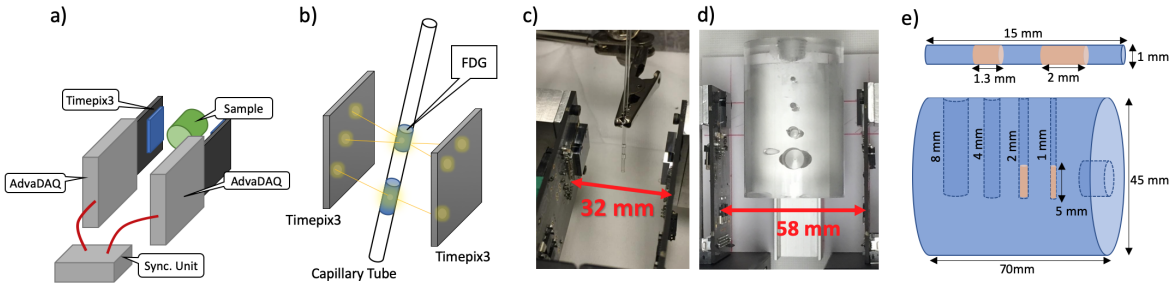

Fig. 4.12: The schema of the detector measurement setup (a). The schema and photo of the measurement with the capillary tube (b, c). The schema and photo of the measurement with phantom (d, e).

Two samples were chosen for the study - a capillary tube and a PMMA phantom with cavities (see figure 4.12). Both samples were filled with a solution of FDG (fludeoxyglucose ^{18}F) that is standardly used radiotracer in PET imaging. The sample were positioned in between the two Timepix3 detectors and gammas emitted from the annihilation of positrons recorded.

4.3.2 Data processing and image reconstruction

The measured data from both Timepix3 detectors were processed - raw ToT values were converted to energy by per-pixel energy calibration, ToA data were corrected for Time-walk effect and the clusters were recognized by the clustering algorithm. The PET principle is based on the coincidence detection of two gammas emitted from a positron annihilation

traveling in the opposite directions. Therefore, the cluster's timestamps (ToA) were compared and coincidence events searched. The events were marked as coincident if they fell into a coincidence time window (see figure 4.13). The size of this time window was determined from the charge collection time of the 2 mm thick CdTe sensor, which was bout 85 ns.

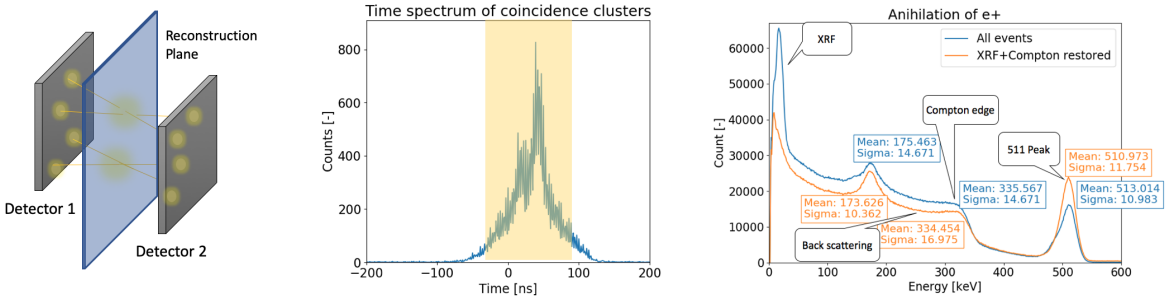

Fig. 4.13: A schema of the image reconstruction (left). Histogram of time differences for coincidence clusters with highlighted coincidence window (middle). Energy spectrum with XRF and Compton reconstruction (right).

The centroids of every two coincidence clusters (one from each detector) were connected with a calculated virtual line. Intersection of the lines with a reconstruction plane were found (see figure 4.13). Several reconstruction planes with different position between the two detectors were generated. The plane in the middle of the measured samples were chosen for further analysis.

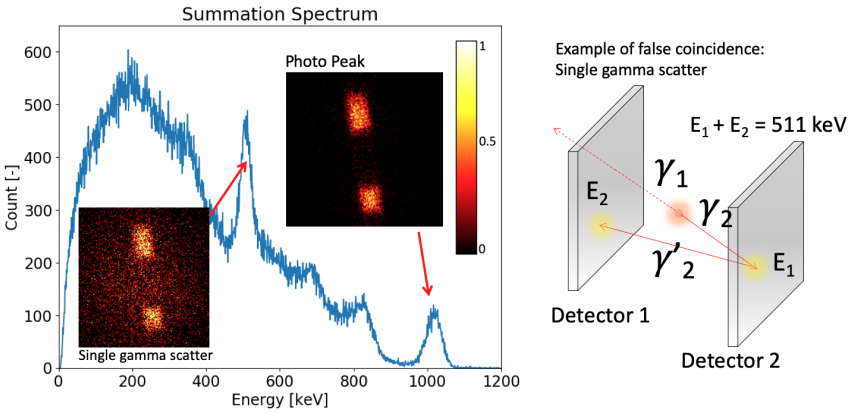

Fig. 4.14: Summation spectrum of coincidence clusters and sample images reconstructed in two selected energy ranges (left). A schema of an example of false coincidence (right).

Similarly as in the case of SPECT measurement, the energy spectrum is affected by the unwanted effects in the CdTe sensors - XRF and Compton scattering. These effect were corrected with the same algorithm as in the SPECT measurement (see figure 4.13 right) and the quality of the energy spectrum and images were improved. The last step in the data processing was the energy filtration (energy cuts). The coincidence events were sorted into groups based on the energy window conditions. The figure 4.14 shows the summation energy spectrum of the coincidence events. The peak at 1022 keV (photo peak) represents the valid coincidence events where each of the two events deposited 511 keV in each detector. It can be seen in

the image generated from these events that there is almost no background signal from XRF and Compton scattering. The rest of the signal outside the photo peak was caused mostly by Compton scattering. The peak around 511 keV represents the case of a false coincidences - when a one of the gamma passes through the first detector, not depositing any charge, the second gamma is scattered in the second detector and it hits the first detector (see figure 4.14 right).

4.3.3 Results

The first measurement sample was a capillary tube filled with 2 droplets of FDG solution. The reconstruction plane was positioned in the middle of the capillary tube. The reconstructed image (see figure 4.15) was calculated from the intersection of lines connecting coincidence clusters. The two droplets are clearly visible in the image. After applying the energy cuts the image contrast improves and the background signal is significantly suppressed (see figure 4.15 middle). The energy cuts not only improves the contrast of the image but also the edges of the areas with the FDG (see figure 4.15 right).

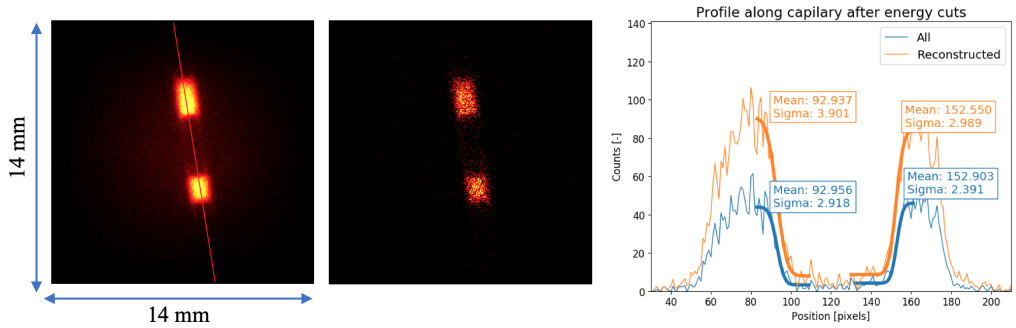

Fig. 4.15: Reconstructed image of the capillary tube filled with 2 droplets of FDG solution (left). Image after after energy filtering - only events from the photo peak) (middle). Profile along the capillary tube (the red line in left image) with fitted edges after energy cuts (right).

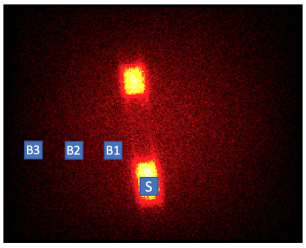

Fig. 4.16: Image areas for BSR analysis.

ROI	BSR_1	BSR_2	BSR_3
All Events	9.8 %	6.9 %	3.4 %
Photo peak	0.37 %	0.12 %	0.03 %
Improvement	26.4	56.2	99.2

Tab. 4.2: Comparing BSR in different areas in the images with different energy cuts.

To quantify the improvements in the images quality, the background to signal ratio (BSR) was used. It is a ratio between an average signal in the background area to an average signal in the area with presence of the FDG. The BSR was calculated for 3 different areas in the background from closest to more distant, from the area containing FDG (see figure 4.16). It is visible that thanks to the energy cuts, it is possible to significantly reduce the background signal. The table 4.2 summaries the BSR calculated for 3 background areas and for the case of applied and not

applied energy filtering. The BSR for the most distant area and the energy filtered events (only from photo peak) is 100 times better.

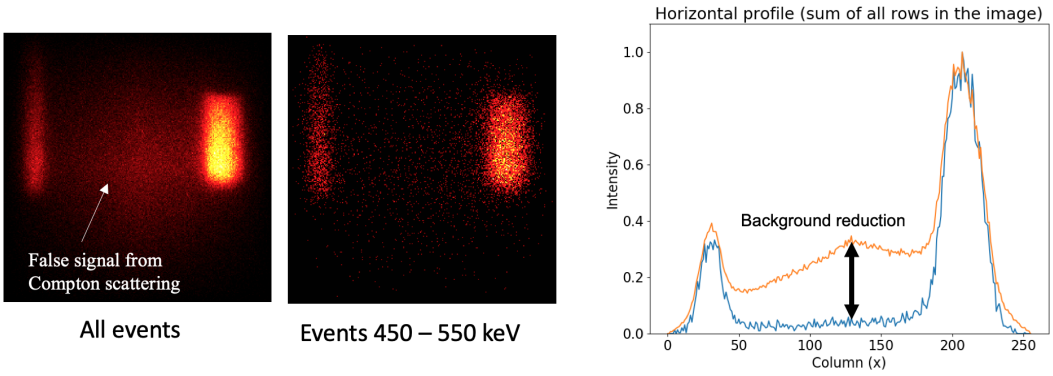

Fig. 4.17: Reconstructed image of the phantom from all the coincidence events (left). Reconstructed image from the photo peak events (middle). Horizontal profile of the both images normalized to the maximum (right). Orange line represents the all events and blue line the photo peak image profile. The massive background reduction is clearly visible.

The second sample - PMMA phantom with cavities was processed in the same way as the first sample. The reconstructed images were again calculated for all events and the energy filtered events (see figure 4.17). The unfiltered image contains relatively large amount of background signal between the two cavities (in the middle of the image). This background signal is caused mostly by Compton scattering in the sensors and the sample itself. After the energy cut this background signal is massively reduced (see figure 4.17 middle). This is even more prominent in the horizontal profiles of both images (see figure 4.17 right).

4.3.4 Discussion

This work has shown very promising results of using Timepix3 detector for PET imaging. Although the measurements were performed only with two detectors and in 2D, the principles can be extended into a full 3D PET scanner. Timepix3 precise measurement of ToA helps in identification of the coincidence events. Thanks to the energy measurement the false coincidence events can be detected and removed from the data. Moreover, the energy cuts can improve the image quality. The greatest benefit of using Timepix3 for PET imaging is the ability to suppress the background signal (mainly from Compton scattering) and to improve the signal to background ratio by two orders of magnitude. Especially in the field of small animal imaging this presents a great advantage, because the conventional PET scanners using the time-of-flight techniques do not reach sufficient resolution due to the small sample size. Moreover, the small dimensions of the AdvaDAQ readouts and high portability permits a construction of a very small and portable PET systems for preclinical imaging of small animals.

My contribution in this publication was writing the text of the publication, performing the measurements, developing algorithms for data processing, analysis of the data and evaluation of the results.

4.4 Publication D - Compton camera based on Timepix3 technology

This publication explores use of Timepix3 detector as a gamma or Compton camera. The gamma camera is traditionally used as a detector in nuclear functional medicine (scintigraphy, SPECT). It usually consists of a collimator block with many high aspect ratio holes and a scintillator detector mounted to many PMTs. This arrangement has several disadvantages: large and heavy collimator, limited detection efficiency and narrow field-of-view. The Compton camera is an alternative method that uses Compton scattering principle and does not require a thick collimator and shielding.

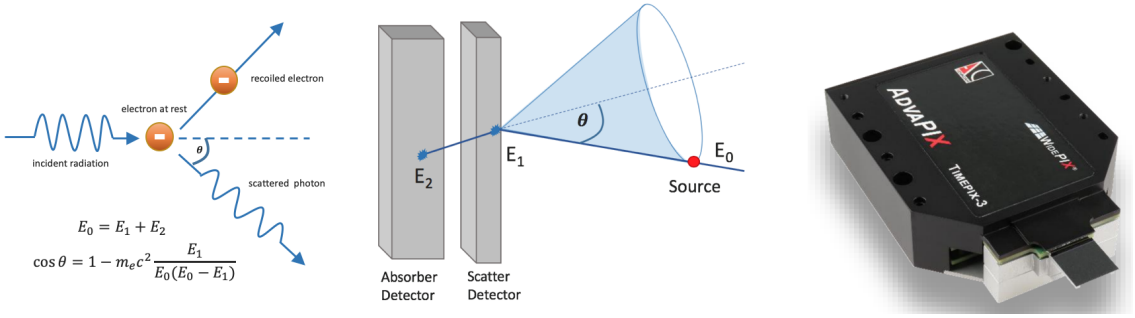

Fig. 4.18: Compton scattering principle (left). Compton camera principle (middle). AdvaPIX readout (right).

The Compton scattering is a scattering of a gamma photon by an electron in a material. When the gamma is scattered, it recoils an electron, loses parts of its energy to this electron and is deflected by the scattering angle θ (see figure 4.18). The scattering angle is depended on the original energy of the gamma and energy of the recoiled electron and can be described by the Compton equation (see figure 4.18).

The Compton camera usually consists of two or more detectors - a scatter detector and the absorbers. The scatter detector scatters the incident gamma photon and records the energy and position of the recoiling electron. The absorber records the energy and position of the scattered gamma photon. From the energies of both events, using Compton equation, it is possible to calculate the scattering angle and estimate the location of the gamma source on a surface of a cone (see figure 4.18). From multiple interaction the location of the gamma source can be determined as an intersection of the cones.

4.4.1 Experimental Setup and Measurement

For the initial measurements, only two Timepix3 layers were used. Timepix3 chips were equipped with two sensors - 1 mm thick Si sensor for the scatterer layer and 1 mm thick CdTe sensor for the absorber layer. The AdvaPIX detectors were placed on top of each other in the

distance of 8 mm and interconnected via a synchronization cable to ensure simultaneous ToA measurement. As a gamma source, a small capillary tube filled with ^{57}Co solution was chosen that emits gamma with energy of 122 keV. The capillary tube was positioned on top of the detectors in a distance of 25 mm at four different lateral positions (see figure 4.19).

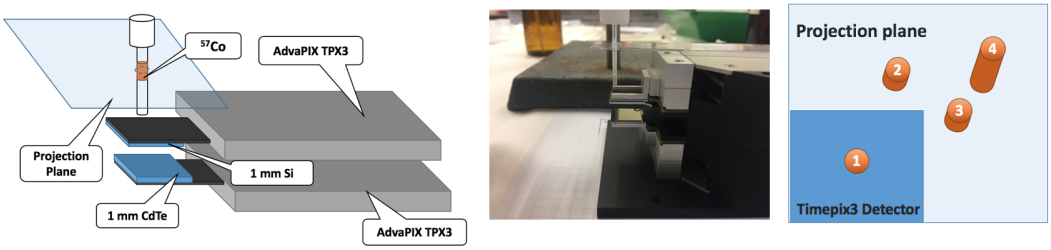

Fig. 4.19: Schema of the measurement setup with 2 AdvaPIX devices and capillary tube (left). Photo of the setup (middle). Top view of the gamma source at 4 different positions (right).

4.4.2 Data processing and reconstruction of the source position

The AdvaPIX detectors were both measuring simultaneously, recording ToA and energy of each incident photon. The measured raw ToT pixel data was converted to energy by per-pixel calibration, ToA was corrected for time-walk effect and the pixel data was analyzed for clusters. The quality of the energy spectrum (see figure 4.20) was affected by internal XRF effect, which was corrected by the correction algorithm similarly as in SPECT and PET measurements. The figure 4.20 right shows the summation spectrum of coincidence events. To improve the results, only events with summation energy around the expected 122 keV peak were selected. The other signal was most likely caused by random coincidences.

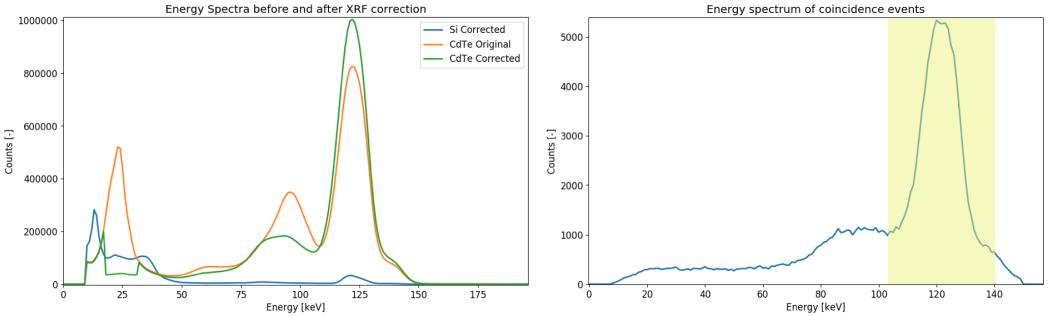

Fig. 4.20: Energy spectrum from Si and CdTe detector before and after application of the internal XRF corrections (left). Energy spectrum of coincidence events with selected energy range for further processing (right).

The filtered coincidence events were further processed and only coincidences containing two events were used for further processing. The 3 and more coincidences could have been caused by random coincidences or multiple Compton scattering, but were ignored for this initial study. The valid events were then inputted into the Compton equation and the scattering angle calculated. From the angle and position of the events in the detectors, a cone was reconstructed

for each coincidence pair. Several projection planes were positioned at different heights on top of the detector and the intersections of multiple cones with these projection planes were calculated (see figure 4.21). From high number of such processed events the position of the gamma source was reconstructed.

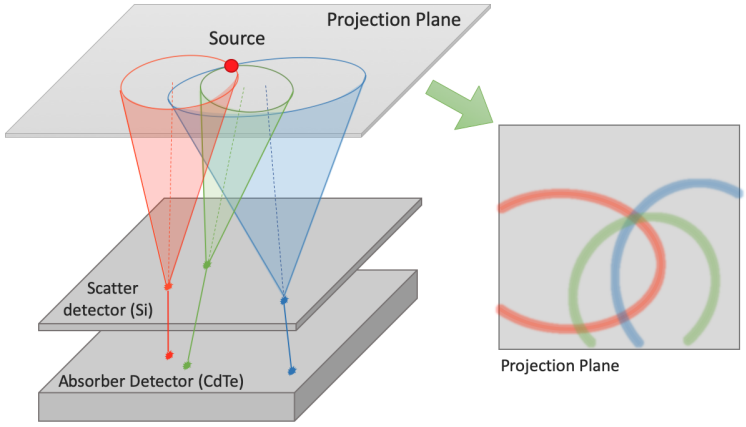

Fig. 4.21: Schema of gamma source position reconstruction. Multiple cones intersecting the projection plane, creating conic curves. The position of the source is located in the intersection of these curves.

4.4.3 Results

The figure 4.22 shows images for the first position of the gamma source, reconstructed from different number of coincidence events. The first image is just an example created from 4 selectively chosen events to demonstrate the principle. For the second image first 1000 coincidence events were taken from the data and after application of the energy filtration only 74 were actually used for the reconstruction. Even from this small amount of events, the gamma source is clearly visible. With the increasing number of events the shape and position of the source is more clear.

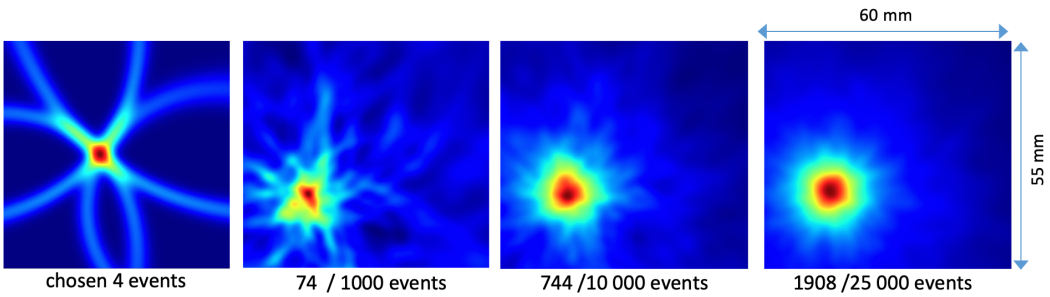

Fig. 4.22: Reconstruction of 4 selected events for demonstration (left). Reconstruction of images from different number of events - first number represents used events after energy filtering, the second number total number of events.

The same reconstruction procedure was done for the other 3 measured gamma source positions (see figure 4.23). For each image, first 100 000 events were taken and, after filtration, less

than 10000 were actually used for reconstruction. All four locations of the gamma source can be clearly seen in the images. The deformation of the fourth position is caused by the inclined geometry (the source was not a point source, but a tall cylinder).

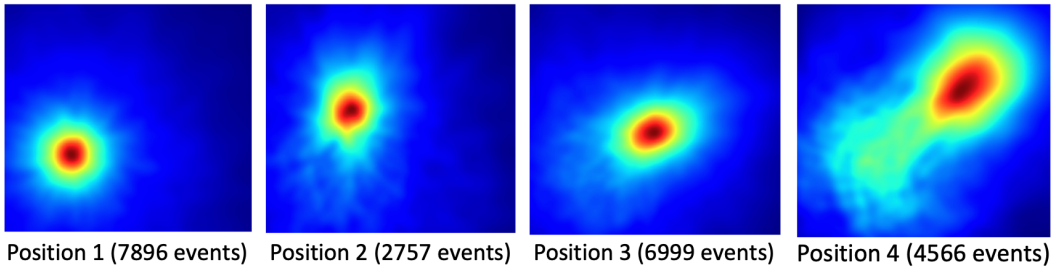

Fig. 4.23: Reconstruction of 4 different gamma source positions.

The quality of the images can be significantly improved by filtering, by application of a deconvolution filter. To be able to create such a filter, a knowledge of the detector response to an ideal point source (point spread function (PSF)) is required. Therefore, a simulation of the Compton camera and a point gamma source with energy of 122 keV was created in order to generate the PSF (see figure 4.24) and calculate the deconvolution filter.

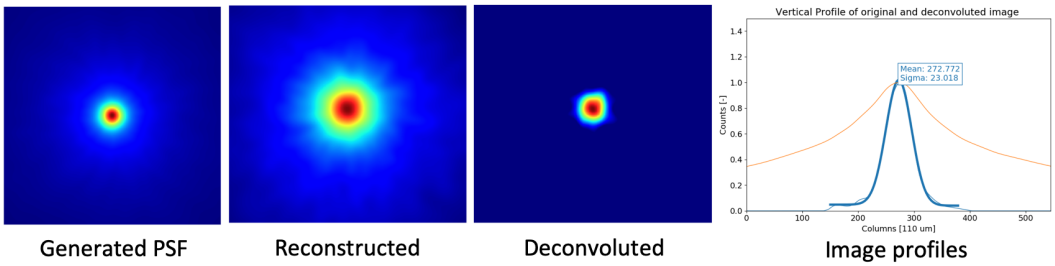

Fig. 4.24: Generated point spread function (left). Original reconstructed image and image after application of the deconvolution filter (middle). Improvement in the image profile before and after deconvolution (right).

Application of the filter on the measured images shows significant image quality improvement. The background signal around the sources was largely suppressed. The figure 4.25 shows the reconstructed images from the 4 positions of the source after application of the deconvolution filter.

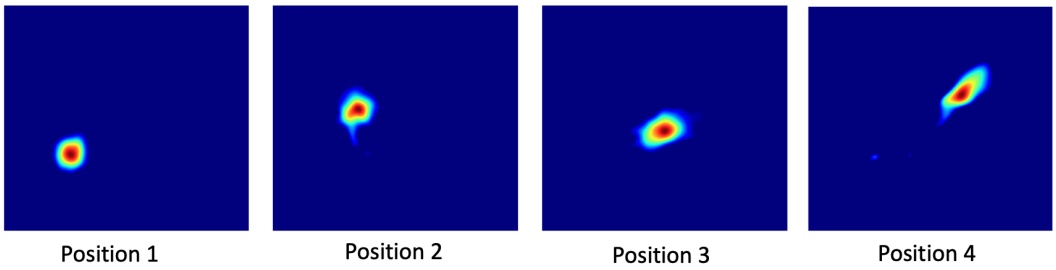

Fig. 4.25: Reconstructed images of 4 source positions after application of the deconvolution filter.

The Compton camera principle was tested in the first measurements only with a single gamma source placed at different locations. In order to verify that the methods works also for multiple gamma sources, four sources were positioned at the same locations as in the previous measurements and the data from all the sources was recorded simultaneously. The figure 4.26 shows results of the measurements before and after application of the deconvolution filter. It is clearly visible that the sources are distinguished. The fourth source is again deformed due to the geometry reasons.

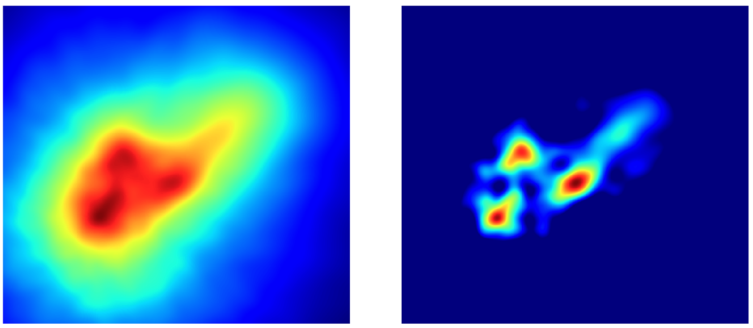

Fig. 4.26: Reconstructed image of multiple gamma sources (left). Deconvoluted image (right).

4.4.4 Discussion

This work demonstrates that the Timepix3 detector can be used for construction of a Compton camera. The methods and algorithms were developed that can reconstruct shape and location of a gamma source from coincidence data measured with two Timepix3 detectors. The principles were tested in measurements with a 122 keV gamma source. The resulting images offer an excellent image resolution of 2 mm, better than the currently available gamma cameras.

Timepix3 based Compton camera offers many benefits over conventional gamma cameras: it does not require usage of a heavy thick shielding and collimator. Therefore it can offer much broader field of view and higher detection efficiency. The camera is also very light, compact and portable. The Compton camera can be used in many imaging modalities (scintigraphy, SPECT, etc.) Because of the small dimension and weight it can massively improve the image quality in the applications were it is necessary to get as close as possible to the sample. An example of such application is a scintigraphy of thyroid gland, where it could reveal small residues after surgical removal of thyroid gland. Localization of such residues helps in preventing further spreading of the cancer cells. There are many other applications that can benefit from the advantages of Timepix3 Compton camera. For example, using multiple Timepix3 detectors in a ring layout, a very small and portable SPECT scanner can be constructed that can be used for preclinical imaging of small animals.

My contribution in this publication was writing the text of the publication, performing the measurements, developing algorithms for data processing, analysis of the data and evaluation of the results.

4.5 Single layer Timepix3 Compton Camera

The aim of this publication is to further explore the Timepix3 detector's usage as the Compton camera. In the previous publication, a multi layer Timepix3 Compton camera was presented. Since the Timepix3 can measured time of arrival (ToA) very precisely (1.56 ns) it is possible to measure charge time collection in the sensors. This knowledge can be used to determine the depth of the interactions in the sensor and thus create a single layer Timepix3 Compton camera. Combined with a new miniaturized readout interface MiniPIX TPX3, a very light, compact single layer Timepix3 Compton camera can be constructed.

4.5.1 Single layer Compton Camera Principle

The principle of the multilayer Compton camera was described in the previous publication. The first detector (scatterer) scatters the incident gamma photon resulting in recoiled electron and gamma photon with reduced energy and changed direction described by Compton equation. This scattered gamma photon then continues towards the second detector (absorber) where it is absorbed. The scattering of the primary gamma and absorption of both the recoiled electron and scattered gamma can often occur within a single detector. Provided that it is possible to determine the depth of these interaction, the scattering angle can be calculated from the Compton equation, the Compton cones constructed and the gamma source localized, similarly as in the case of multi layer Compton camera.

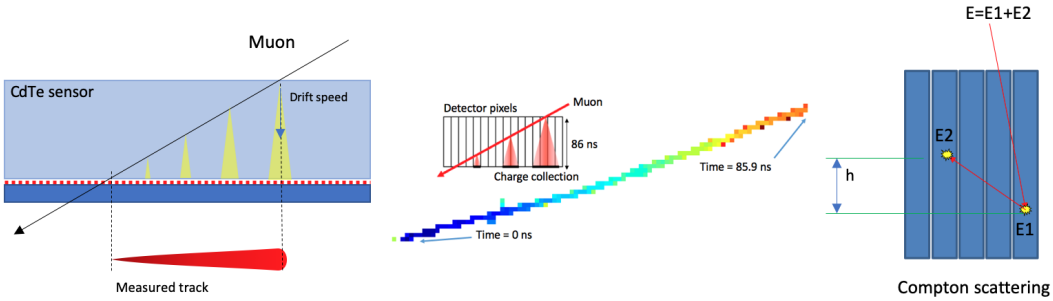

Fig. 4.27: Schema of the charge collection in the sensor for a muon track (left). Example of a measured muon track with total charge collection time (middle). Schema of the Compton scattering within a sensor (right).

The depth of the interaction can be determined from the charge collection time in the sensor. The events that interact closer to the top part of the sensor takes longer time to be collected than the events interacting closer to the bottom (see figure 4.27). The charge collection time is proportional to the depth. To convert the time to the depth, a knowledge of the total charge collection time through the whole detector thickness is necessary. This can be obtained from a measurement with cosmic muons. The muons penetrate the whole detector thickness and the time difference between the first and last pixel in the recorded track is the total charge collection time. For the 2 mm thick CdTe sensor this time is about 86 ns.

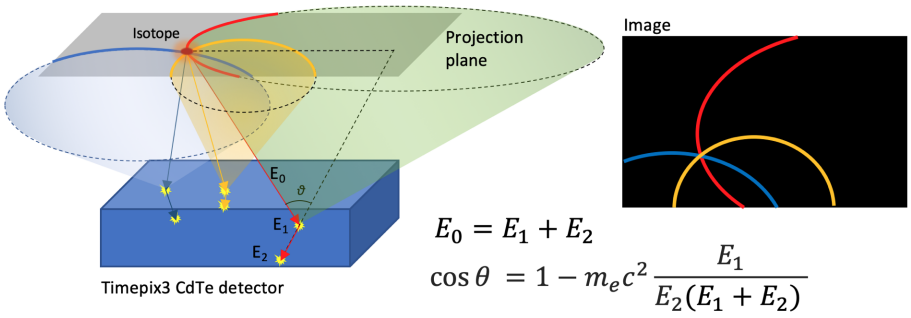

Fig. 4.28: Schema of the reconstruction of gamma source position (left). Reconstructed image (right). Calculation of the scattering angle from Compton equation (middle).

For both of the Compton scattering events (recoiled electron and scattered gamma) the time is measured and the difference of these times converted to the difference in depth. The 2D location is known from the position of hit pixels and energy from their recorded values. Therefore, full 3D position is known and the scattering angle can be calculated from the Compton equation. From the angles, cones are constructed and their intersection with a projection plane (conic curves) plotted (see figure 4.28). From multiple events the position of the gamma source is located in the intersection of the conic curves in the projection plane.

4.5.2 Miniaturized Readout Interface MiniPIX TPX3

The Minipix TPX3 (see figure 4.29) was developed in order to have a miniaturized, compact, simplified and cheaper version of the AdvaPIX TPX3 detector. It was designed for wide range of imaging and particle tracking applications including the Compton camera application. It is a USB stick size device with USB 2.0 connectivity that offers a maximal hit rage of 2.3 million hits/s/cm^2 in event by event mode. It can be equipped with different sensors (Si, CdTe, CZT) and can supply biasing voltages from - 500 V to 300 V.

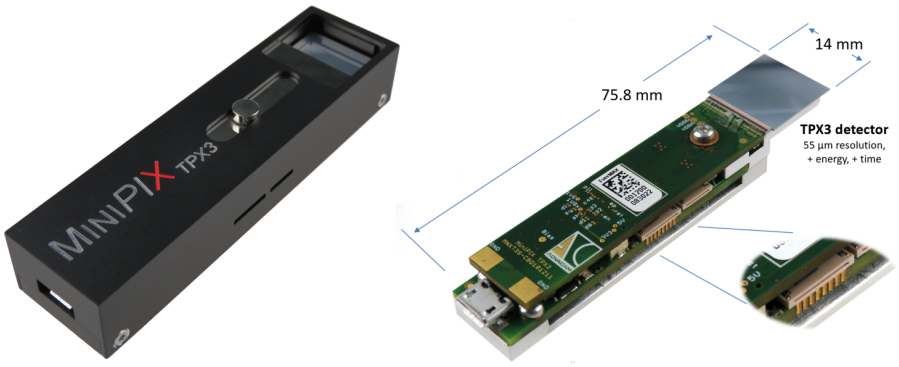

Fig. 4.29: Photo of the MiniPIX TPX3 readout device. Photo of the internal PCB inside MiniPIX TPX3 with dimensions.

4.5.3 Measurement with Ba source

The principles of the single layer Compton camera were verified by several measurements. The first experiment was a measurement with ^{133}Ba source. ^{133}Ba gamma source was dissolved in a silicon and cut into small cubes of about 3 mm x 3 mmm size. These were positioned on top of the detector in the distance of 2 cm (see figure 4.30). The measured data were processed and a back-projection image calculated (see figure 4.30). All four sources were clearly recognized. The differences in the intensities of each source in the image are caused by the different volumes of each cube.

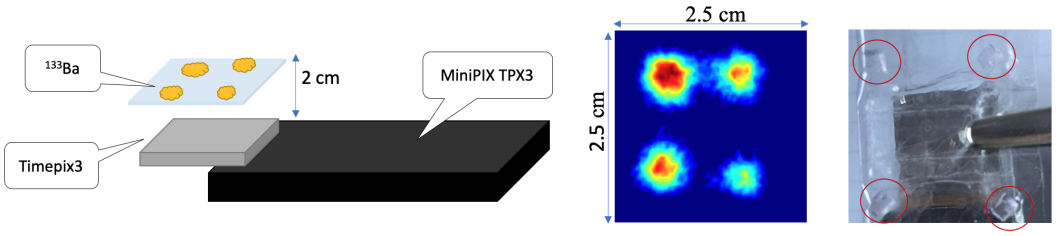

Fig. 4.30: Schema of the measurement setup (left). Reconstructed image (middle). Photo of the measurement setup (right).

4.5.4 Measurement with Multiple sources

The second measurement was done with multiple gamma sources with different energies: iodine (^{131}I, 364 keV), sodium (^{22}Na, 511 keV) and cesium (^{137}Cs, 662 keV). The sources were placed on top of the detector in the distance of 7 cm (see figure 4.31). The energy spectrum was created that shows peaks from all the 3 sources (see figure 4.31). All 3 sources are also recognized in the back-projected image.

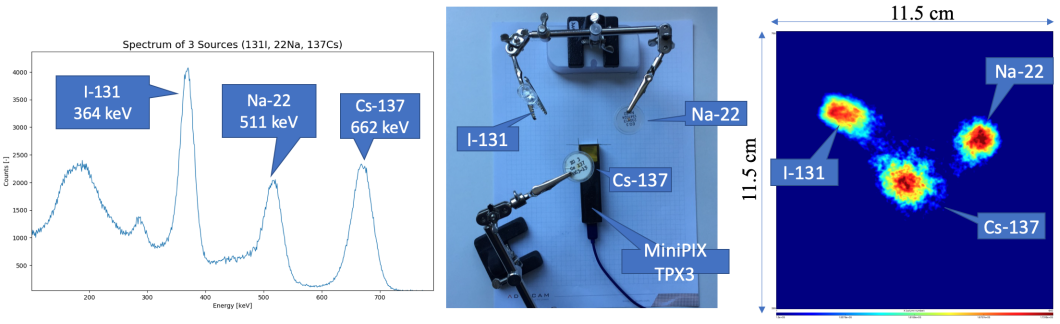

Fig. 4.31: Energy spectrum of measurement with multiple gamma sources (left). Photo of the measurement setup (middle). Back-projected image of the sources (right).

The 3 sources are distinctively recognizable in the energy spectrum (see figure 4.31). Therefore, it should be possible to separate them reconstruction process and resulting images. The measured data were separated into several energy windows of 50 keV width covering the energy range from 0 to 750 keV (see figure 4.32). Each energy window's data were processed and corresponding image reconstructed (see figure 4.32). The images show that the gamma

sources were clearly separated - in each energy window there is either no data or corresponding gamma source. The energy bin 250 - 300 keV also shows a signal. This is a second energy peak from ^{131}I source, which has a low probability (only 7 %).

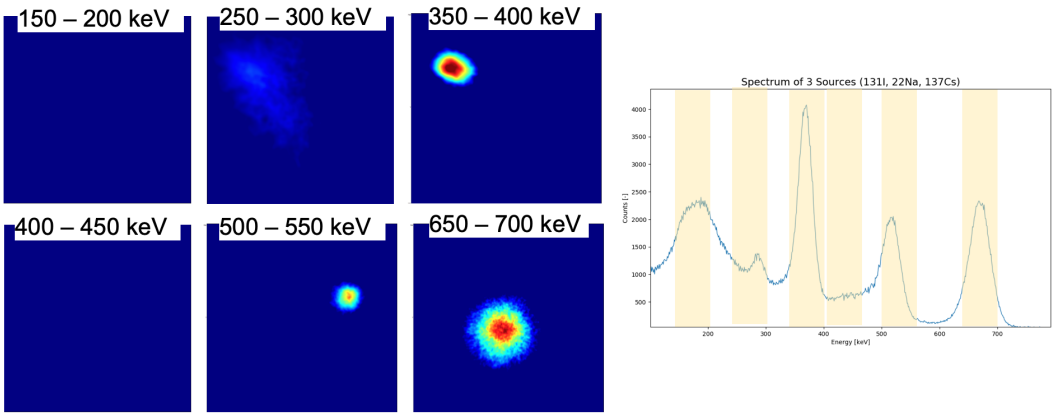

Fig. 4.32: Reconstructed images for multiple energy windows (left) and the energy spectrum with highlighted energy windows (right).

This measurement demonstrated that the single layer Timepix3 Compton camera is not only able to localize different gamma sources but also to recognize the different types of sources by their energy.

4.5.5 Measurement with gamma sources in an environment

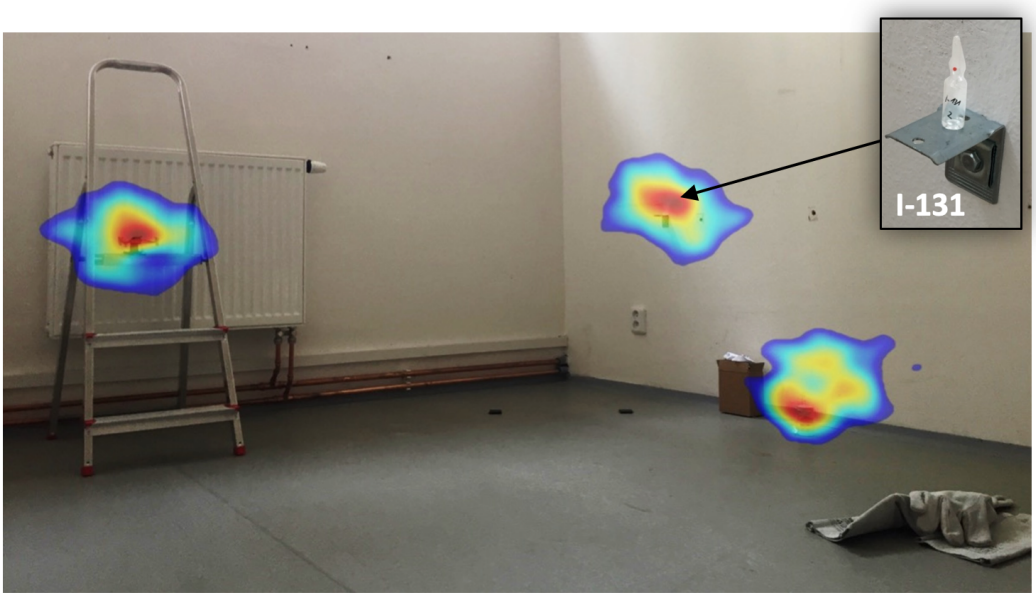

Fig. 4.33: Photo of a room with 3 gamma sources at different positions combined with the reconstructed image.

The goal of the last measurement was to test the Compton camera with sources placed in an environment in larger distances from the detector. Three flasks filled with ^{131}I solution were placed in a room at different locations in the distance of about 3 m from the detector (see figure 4.33). The measured data were processed and the image with location of the sources reconstructed. The image was combined with a photo of the room taken from the point of view of the detector, keeping the correct proportions (see figure 4.33). All three sources were correctly recognized.

4.5.6 Discussion

This work represents the continuation of the efforts in Timepix3 Compton camera concept. The previous publication explored the possibility of using multiple Timepix3 detector layers as Compton camera, whereas this work explores possibility of improving on the previous design by using just a single Timepix3 detector. Thanks to Timepix3 high time resolution of 1.56 ns, it is possible to measure time of charge collection within the sensor, which can be converted into depth information. By combining the Timepix3 detector with a new miniaturized readout interface MiniPIX TPX3, it possible to construct a very compact, light and flexible single layer Timepix3 Compton camera.

The principle of the single layer Compton camera was verified on several measurements with different gamma sources. The sources were positioned close and further from the detector. Multiple different sources were measured at the same time. The device is not only capable of locating a gamma source but also, based on the energy, distinguish different types of sources. Thanks to its even smaller dimensions that the previous AdvaPIX TPX3 based Compton camera, it is possible to use it new applications were the size and weight of the detectors matters. One of such application could be the location of radioactive isotopes in an environment using drones equipped with this Compton camera, where the minimal dimensions and weight of the detectors is crucial.

My contribution in this publication was writing the text of the publication, performing the measurements, developing algorithms for data processing, analysis of the data and evaluation of the results.

5 Conclusion

Medical imaging is nowadays a very important medical diagnostic tool and the imaging using ionizing radiation is a rapidly developing field. The novel imaging detectors with their advance parameters and features can bring significant improvements in the image quality in the medical imaging and can even open entirely new applications. This work was focused on the state of the art hybrid single photon counting pixel detectors of the Medipix family, mainly the newest detector Timepix3. This detector has promising features such as simultaneous measurement of the energy and time of arrival of the incident photons in each pixel. The aim of this work was therefore to explore the features of this detector and its applicability in different medical imaging modalities.

At first the necessary infrastructure, a readout hardware and software, was created that made it possible to operate and characterize the detector and find its limits in the sense of measurement of the energy and time. Then, each modality of Timepix3 was successively explored. First, the photon counting was evaluated in very fast radiographic measurements, where usage of Timepix3 brought not only high frame rates but also higher spatial resolution and less noise in the images. Then, the energy modality was explored. The energy information was useful in reconstruction of the energy spectra and improvement of the image quality by suppression of the unwanted signal from the intrinsic effects of the sensors such as internal X-ray fluorescence or Compton scattering. These techniques were then used in SPECT imaging application, where it helped significantly in reduction of the background signal. Further, the time measurement was studied and a technique was developed that recognizes various coincidence events. This technique allowed us to recognize coincidence gamma events from positron annihilation in PET imaging application. Last but not least, the usage of both time and energy information at the same time was investigated in the multi-layer Compton camera concept, where it allowed recognition of the Compton scattering events and reconstruction of the positions of gamma sources. By further improving the Compton camera and utilizing the full time resolution of Timepix3 detector, it was possible to create a Compton camera in a single monolithic detector, a new groundbreaking principle that was not possible before. The small dimensions of the Timepix3 detector lead us to the idea of designing a miniaturized readout interface MiniPIX TPX3, thus creating the world's smallest and lightest Compton/Gamma camera in the size of a USB flash stick and weight of only 15 grams.

All the work presented in this thesis demonstrated the great potential of single photon counting detectors such as Timepix3 in medical imaging. This work has created the infrastructure and conditions for use of these detectors in many new imaging applications. Several new projects has been already started based on the results of this work:

- Diagnostic of thyroid gland - because of the small dimension of the MiniPIX TPX3 Compton camera and no need for the collimators and shielding, it will be possible to reduce significantly the dose received by the patients and at the same time improve the resolution of the images.

- Detection of isotopes in an environment - thanks to the small dimensions and weight of the MiniPIX TPX3 Compton camera, it is possible to mount the camera to autonomous drones that would localize different sources in an environment

- Space application - usage of the MiniPIX TPX3 camera as a miniaturized dosimeter for space conditions

The results in this work represent the proof-of-concepts and first studies. In the future, these concepts will be further studied and improved. Also, the development of the single photon counting detectors has not stopped and new detectors with more advanced features are being designed. Timepix4, a successor detector to Timepix3 chip, is being finalized at CERN. This detector will bring 4 times larger area and will offer time resolution of 200 ps, 8 times better than the current Timepix3 detector. It is clear, that the single photon counting pixel detectors have a great potential for the future not only in medical imaging but in many other applications.

Bibliography

Adler, Arlene and Richard Carlton (2016). *Introduction to radiologic & imaging sciences & patient care*. eng. Sixth edition.. (cit. on p. 16).

Als-Nielsen, J. and D. McMorrow (2011). *Elements of Modern X-ray Physics*. Wiley (cit. on p. 18).

ARPANSA (2019). *X-rays*. URL: https://www.arpansa.gov.au/understanding-radiation/what-is-radiation/ionising-radiation/x-ray (visited on July 10, 2019) (cit. on p. 18).

Ballabriga, R., M. Campbell, H. Heijne, et al. (2011). „Medipix3: A 64k pixel detector readout chip working in single photon counting mode with improved spectrometric performance“. In: *Nuclear Instruments and Methods in Physics Research Section A* 633, pp. 15–18 (cit. on p. 42).

Behling, Rolf (2015). *Modern Diagnostic X-Ray Sources, Technology, Manufacturing, Reliability*. eng. CRC Press (cit. on p. 17).

Binns, D.S. (2001). „Recent Advances in Nuclear Medicine Imaging Technology“. In: (cit. on p. 29).

Blue-Optics (2019). *Ce:YAG crystal*. URL: http://blueoptics.cn/products/scintillation/2014/0929/11.html (visited on Aug. 10, 2019) (cit. on p. 31).

Campbell, M. and al. (1998). „A readout chip for a 64 x 64 pixel matrix with 15-bit single photon counting“. In: *IEE Transactions on Nuclear Science* 45 (cit. on p. 39).

Cantatore, A. and P Muller (2011). „Introduction to computed tomography“. In: *DTU Mechanical Engineering* (cit. on p. 24).

Carroll, Q.B. (2014). *Radiography in the Digital Age: Physics - Exposure - Radiation Biology*. Charles C. Thomas, Publisher, Limited (cit. on p. 16).

Cerrito, L. (2018). *Radiation and Detectors: Introduction to the Physics of Radiation and Detection Devices*. Graduate Texts in Physics. Springer International Publishing (cit. on p. 30).

Cervantes, Guillermo Avendaño (2016). „X-ray tubes“. In: *Technical Fundamentals of Radiology and CT*. 2053-2563. IOP Publishing, 5–1 to 5–16 (cit. on p. 18).

Development of large-volume high-performance monolithic CZT radiation detector (2018). Vol. 10762 (cit. on p. 38).

Delpierre, P (2014). „A history of hybrid pixel detectors, from high energy physics to medical imaging“. In: *Journal of Instrumentation* 9.05, pp. C05059–C05059 (cit. on p. 37).

E. Kotter, M. Langer (2002). *Digital radiography with large-area flat-panel detectors*. Springer (cit. on pp. 34, 35).

Feege, N. (2008). *Silicon Photomultipliers: Properties and Application in a Highly Granular Calorimeter*. DESY thesis. DESY (cit. on p. 34).

Flyckt S.O., Marmonier C. (2002). *Photomultiplier tubes: Principles and Applications*. Philips Photonics (cit. on p. 32).

Förster, Andreas, Stefan Brandstetter, and Clemens Schulze-Briese (2019). „Transforming X-ray detection with hybrid photon counting detectors“. In: *Philosophical Transactions of the Royal Society A: Mathematical, Physical and Engineering Sciences* 377.2147, p. 20180241. eprint: `https://royalsocietypublishing.org/doi/pdf/10.1098/rsta.2018.0241` (cit. on p. 37).

GE (2019). *Optima NM/CT 640*. URL: `https://www.gehealthcare.com` (visited on July 15, 2019) (cit. on p. 25).

Granov, A., L. Tiutin, and T. Schwarz (2013). *Positron Emission Tomography*. Springer Berlin Heidelberg (cit. on p. 27).

Hani, A.F.M. and D. Kumar (2017). *Optical Imaging for Biomedical and Clinical Applications*. CRC Press (cit. on p. 13).

Heidekker, Mark A (2013). *Medical Imaging Technology*. eng. Springer (cit. on pp. 13, 20, 25).

Heijne, E.H.M. (1988). „The silicon micropattern detector: A dream ?“ In: *Nuclear Instruments and Methods in Physics Research Section A* 273, pp. 615–619 (cit. on p. 37).

Heijne, E.H.M. (1994). „Development of silicon micropattern pixel detectors“. In: *Nuclear Instruments and Methods in Physics Research Section A* 348, pp. 399–408 (cit. on p. 37).

Horrocks, D. (2012). *Organic Scintillators and Scintillation Counting*. Elsevier Science (cit. on p. 31).

Jakubek, Jan (2009). „Semiconductor Pixet Detectors and their Applications in Life Sciences“. In: *Journal of Instrumentation* 4 (cit. on p. 39).

Jakubek, Jan (2011). „Precise energy calibration of pixel detector working in time-over-threshold mode“. In: *Nucler Instruments and Methods in Physics Research Section A* 633, pp. 262–266 (cit. on p. 42).

Jakubek, Jan and Martin Kroupa (2011). „X-ray phase constrast imaging using absorption coded aperture“. In: *Nucler Instruments and Methods in Physics Research Section A* (cit. on p. 42).

Johnston, James N. and Terri L. Fauber. (2016). *Essentials of radiographic physics and imaging*. eng. Elsevier (cit. on pp. 17, 23).

Kalender, W.A. (2011). *Computed Tomography: Fundamentals, System Technology, Image Quality, Applications*. Wiley (cit. on p. 21).

Knoll, Glenn F (2000). *Radiation Detection and Measurement, 3rd edition*. Wiley (cit. on pp. 31, 33).

Knopp, T. and T.M. Buzug (2012). *Magnetic Particle Imaging: An Introduction to Imaging Principles and Scanner Instrumentation*. Springer Berlin Heidelberg (cit. on p. 14).

Korzhik, M. and A. Gektin (2017). *Engineering of Scintillation Materials and Radiation Technologies: Proceedings of ISMART 2016*. Springer Proceedings in Physics. Springer International Publishing (cit. on p. 30).

Lawson, R.S., C. Tonge, W.A. Waddington, et al. (2013). *The Gamma Camera: A Comprehensive Guide*. Institution of Physics & Engineering in Medicine & Biology (cit. on p. 26).

Llopart, X., M. Campbell, D. San Segundo, E. Pernigotti, and R. Dinapoli (2001). „Medipix2, a 64k pixel read out chip with 55 /spl mu/m square elements working in single photon counting mode“. In: *2001 IEEE Nuclear Science Symposium Conference Record (Cat. No.01CH37310)*. Vol. 3, 1484–1488 vol.3 (cit. on pp. 39–41).

Llopart, X., R. Ballabriga, M. Campbell, L. Tlustos, and W. Wong (2007). „Timepix, a 65k programmable pixel readout chip for arrival time, energy and/or photon counting measurements“. In: *Nucl. Instrum. Meth.* A581. [Erratum: Nucl. Instrum. Meth.A585,106(2008)], pp. 485–494 (cit. on p. 41).

Luna, A., J.C. Vilanova, L.C.H. Da Cruz, and S.E. Rossi (2014). *Functional Imaging in Oncology: Clinical Applications* -. sv. 2. Springer Berlin Heidelberg (cit. on p. 15).

M. Langer, E. Kotter (2003). „Digital radiography with large-area flat-panel detectors“. In: *European Radiology* 12.10, pp. 2562–2570 (cit. on p. 35).

Macmilian (2019). *CT scan (computerised tomography)*. URL: https://www.macmillan.org.uk/information-and-support/diagnosing/how-cancers-are-diagnosed/tests-and-scans/ct-scan.html (visited on July 11, 2019) (cit. on p. 20).

Martz, H.E., C.M. Logan, D.J. Schneberk, and P.J. Shull (2016). *X-Ray Imaging: Fundamentals, Industrial Techniques and Applications*. CRC Press (cit. on p. 15).

Medipix Collaboration (2019). *Medipix Collaboration Web Page*. URL: https://medipix.web.cern.ch/ (visited on June 27, 2019) (cit. on pp. 39, 44).

Moroder, Wolfgang (2019). *Ultrasound image of a fetus in the womb*. URL: https://en.wikipedia.org/wiki/Ultrasound (visited on Sept. 10, 2019) (cit. on p. 14).

Nakamoto, D., N. Azar, C. Donaldson, and V. Dogra (2015). *RadCases Ultrasound Imaging*. Radcases Plus Q&a Series. Thieme (cit. on p. 14).

National Cancer Institute (2019). *NCI Dictionary of Cancer Terms - Bone Scan*. URL: https://www.cancer.gov/publications/dictionaries/cancer-terms/def/bone-scintigraphy (visited on July 10, 2019) (cit. on p. 19).

Platkevič, Michal (2014). „Signal processing and Data Read-out from Position Sensitive Pixel Detectors“. PhD thesis. Czech Technical University (cit. on p. 38).

Poikela, T, J Plosila, T Westerlund, et al. (2014). „Timepix3: a 65K channel hybrid pixel readout chip with simultaneous ToA/ToT and sparse readout“. In: *Journal of Instrumentation* 9.05, pp. C05013–C05013 (cit. on pp. 44–46).

Powsner, R.A. and E.R. Powsner (2006). *Essential Nuclear Medicine Physics*. Essentials. Wiley (cit. on pp. 27, 28).

Radiology, Carolina (2019). *Magnetic Resonance Imaging*. URL: https://carolinaradiology.com/magnetic-resonance-imaging-mri/ (visited on Sept. 10, 2019) (cit. on p. 15).

Romans, L.E. (2011). *Computed Tomography for Technologists: A Comprehensive Text*. Lippincott Williams & Wilkins (cit. on p. 22).

Russell, J. and R. Cohn (2012). *Avalanche Photodiode*. Book on Demand (cit. on p. 34).

Russo, Paolo (2018). *Handbook of X-ray imaging: Physics and Technology*. Taylor and Francis (cit. on pp. 36, 37).

Saha, Gopal B. (2006). *Physics and Radiobiology of Nuclear Medicine*. Springer (cit. on p. 29).

Seibert and J. Anthony (2006). „Flat-panel detectors: how much better are they?“ In: *Pediatric radiology* 36 Suppl 2.Suppl 2. 16862412[pmid], pp. 173–181 (cit. on p. 35).

Seibert, James (Oct. 2006). „Flat-panel detectors: How much better are they?“ In: *Pediatric radiology* 36 Suppl 2, pp. 173–81 (cit. on p. 36).

Seitz, P. and A.J.P. Theuwissen (2011). *Single-Photon Imaging*. Springer Series in Optical Sciences. Springer Berlin Heidelberg (cit. on p. 37).

Semiconductor, ON (2018). *Application Note - AND9770/D - Introduction to Silicon Photomultiplier (SiMP)*. URL: https://www.onsemi.com/pub/Collateral/AND9770-D.PDF (visited on June 27, 2019) (cit. on p. 34).

SENSE (2019). *Photomultiplier Tubes (PMT)*. URL: https://www.sense-pro.org/lll-sensors/pmt (visited on Aug. 8, 2019) (cit. on p. 32).

Sharp, P.F., H.G. Gemmell, and A.D. Murray (2005). *Practical Nuclear Medicine*. Springer (cit. on pp. 26, 28).

Streba, C. T., B. S. Ungureanu, and C.C. Vere D. I. Gheonea and (2018). „Endoscopy - Novel Techniques and Recent Advancements“. In: *Intechopen* (cit. on p. 13).

Thomas, A.M.K. and A.K. Banerjee (2013). *The History of Radiology*. Oxford Medical Histories. OUP Oxford (cit. on p. 17).

Turecek, D, L Pinsky, J Jakubek, et al. (2011). „Small Dosimeter based on Timepix device for International Space Station“. In: *Journal of Instrumentation* 6.12, pp. C12037–C12037 (cit. on p. 42).

Uher, Josef and Jan Jakubek (2011). „Detection of fast neutrons with particle tracking detector Timepix combined with plastic scintillator“. In: *Radiation Measurements* 46 (cit. on p. 42).

Vallabhajosula, S. (2009). *Molecular Imaging: Radiopharmaceuticals for PET and SPECT*. Springer Berlin Heidelberg (cit. on p. 25).

Vykydal, Zdenek (2004). „USB Interface for Medipix2 Pixel Device Enabling Energy and Position Detection of Heavy Charged Particles“. PhD thesis. Czech Technical University (cit. on p. 40).

Waterstram-Rich, K.M. and D. Gilmore (2016). *Nuclear Medicine and PET/CT - E-Book: Technology and Techniques*. Elsevier Health Sciences (cit. on p. 30).

Weber, M.A. (2013). *Magnetic Resonance Imaging of the Skeletal Musculature*. Medical Radiology. Springer Berlin Heidelberg (cit. on p. 14).

Wikihow (2019). *How to prepare for an Endoscopy*. URL: https://www.wikihow.com/Prepare-for-an-Endoscopy (visited on Sept. 10, 2019) (cit. on p. 13).

Wikipedia (2019). *Bone scintigraphy*. URL: https://en.wikipedia.org/wiki/Bone_scintigraphy (visited on July 10, 2019) (cit. on p. 19).

Yun, I. (2012). *Photodiodes: From Fundamentals to Applications*. IntechOpen (cit. on p. 33).

Zaidi, H. and T. Kwee (2013). *Evolving Medical Imaging Techniques, An Issue of PET Clinics, E-Book*. The Clinics: Radiology. Elsevier Health Sciences (cit. on p. 29).

Zemlicka, Jan, Jan Jakubek, Martin Kroupa, and Vladimir Tichy (2009). „Energy and position sensitive pixel detector Timepix for X-ray fluorescence imaging“. In: *Nucler Instruments and Methods in Physics Research Section A* 607, pp. 202–204 (cit. on p. 42).

Zeng, G. (2010). *Medical Image Reconstruction: A Conceptual Tutorial*. Springer Berlin Heidelberg (cit. on p. 23).

Zou, Chunpeng, Beibei Wu, Yanyan Dong, et al. (Dec. 2016). „Biomedical photoacoustics: Fundamentals, instrumentation and perspectives on nanomedicine“. In: *International Journal of Nanomedicine* Volume 12, pp. 179–195 (cit. on p. 14).

6 Publications

Publications in extenso, that constitute the basis of the PhD thesis:

- Turecek D., Jakubek J., Trojanova E., Sefc L., “Compton camera based on Timepix3 technology“, JINST Vol 13, C11022 (2018) doi: 10.1088/1748-0221/13/11/C11022 (IF=1.366)
- Turecek D., Jakubek J., Trojanova E., Sefc L., Kolarova V., “Application of Timepix3 based CdTe spectral sensitive photon counting detector for PET imaging“., Nuclear Instruments and Methods in Physics Research Section A, Volume 895, p84-89 (2018) doi: 10.1016/j.nima.2018.04.007 (IF=1.433)
- Turecek D., Jakubek J., Soukup P., “USB 3.0 readout and time-walk correction method for Timepix3 detector“, JINST Vol 11, C12065, December 2016, DOI: 10.1088/1748-0221/11/12/C12065 (IF=1.366)
- Khalil M., Turecek D., Jakubek J., Kehres J., Dreier E.S., Olsen U.L., “Intrinsic XRF correction in Timepix3 CdTe spectral detectors”, JINST Vol 14, C01018 (2019), doi: 10.1088/1748-0221/14/01/C01018 (IF=1.366)
- Trojanova, E. Schyns, L.E.J.R. Ludwig, D. Jakubek, J. Pape, A.L. Sefc, L. Lotte, S. Sykora, V. Turecek, D. Uher, J. Verhaegen, F. Tissue sensitive imaging and tomography without contrast agents for small animals with Timepix based detectors. Volume 12, Issue 1, 20 January 2017, Article number C01056, DOI: 10.1088/1748-0221/12/01/C01056, (IF=1.31)
- Trojanova,E. Jakubek, J. Turecek, D. Sykora, V. Francova, P. Kolarova V. and Sefc, L. Evaluation of Timepix3 based CdTe photon counting detector for fully spectroscopic small animal SPECT imaging. JINST, Volume 13, Issue 1, 2 January 2018 (IF=1.366)

Other publications with impact factor in extenso:

- R. Felix-Bautista, T. Gehrke, L. Ghesquiere-Dierick, M. Reimold, C. Amato, D. Turecek, J. Jakubek, M. Ellerbrock and M. Martisikova, "Experimental verification of a non-invasive method to monitor the lateral pencil beam position in an anthropomorphic phantom for carbon-ion radiotherapy" Physics in Medicine and Biology, Vol. 64, Num. 17, doi: 10.1088/1361-6560/ab2ca3 (2019) (IF=3.03)
- George S., Turecek D., Wheeler S., Kodiara S., Pinsky L., "First Test with Timepix2 and Heavy Ions", Nuclear Instruments and Methods Section A, doi: 10.1016/j.nima.2019.162725 (2019) (IF=1.433)

- Dreier E.S., Silvestre C., Kehres J., Turecek D., Khalil M., Hemmingsen J.H., Hansen O., Jakubek J., Feidenhands I., Olsen U.L, “Virtual subpixel approach for single-mask phase-contrast imaging using Timepix3”., JINST Vol 14, C01011 (2019), doi: 10.1088/1748-0221/14/01/C01011 (IF=1.366)

- Campbell M., Heijne E., Leroy C., Nessi M., Pospisil S., Solc J., Suk M., Turecek D., Vykydal Z., "Induced radioactivity in ATLAS cavern measured by MPX detector network" Journal of Instrumentation, Vol 14. 10.1088/1748-0221/14/03/P03010 (2019) (IF=1.366)

- Campbell M., Heijne E., Leroy C., Nessi M., Pospisil S., Solc J., Suk M., Turecek D., Vykydal Z., "Penetration of ionizing radiation from ATLAS cavern into USA15 measured by MPX detectors" Journal of Instrumentation, Vol 14. 10.1088/1748-0221/14/02/P02020 (2019) (IF=1.366)

- Baca T., Turecek D., McEntaffer R., Filgas R., “Rospix: modular software tool for automated data acquisitions of Timepix detectors on Robot Operating System“, JINST Vol 13, C110008 (2018), doi: 10.1088/1748-0221/13/11/C11008/meta (IF=1.366)

- Gehrke T., Burigo L., Arico G., Berke S., Jakubek J., Turecek D., Tessonnier T., Mairani A., Martisikova M., Energy deposition measurements of single H-1, He-4 and C-12 ions of therapeutic energies in a silicon pixel detector. JINST, Volume 12, P04025, Apr 2017. DOI: 10.1088/1748-0221/12/04/P04025. (IF=1.366)

- Gallas R. R., Arico G., Burigo L. N., Gehrke T., Jakubek J., Granja C., Turecek D., Martisikova M. "A novel method for assessment of fragmentation and beam-material interactions in helium ion radiotherapy with a miniaturized setup", Physica Medica - European Journal of Medical Physics, Vol 42, doi: 10.1016/j.ejmp.2017.09.126 (2017) (IF=2.532)

- Sopczak, A. and Ali, B. and Asbah, N. and Bergmann, Turecek D., et al., "Luminosity from thermal neutron counting with MPX detectors and relation to ATLAS reference luminosity at root s=8 TeV proton-proton collisions", JINST, Vol 12, doi: 10.1088/1748-0221/12/09/P09010 (2017) (IF=1.366)

- Kroupa M., Bahadori A, Campbell-Ricketts T, Turecek D. et al. "A semiconductor radiation imaging pixel detector for space radiation dosimetry." Life sciences in space research Volume: 6 Pages: 69-78 (2015) (IF=2.066)

- N. Stoffle, L. Pinsky, M. Kroupa, D. Turecek, et al., "Timepix-based radiation environment monitor measurements aboard the International Space Station" , Nuclear Instruments and Methods in Physics Research Section A, Volume: 782 Pages: 143-148 (2015) (IF=1.433)

- Fila, T.; Kumpova, I.; Jandejsek, I.; Turecek D. et al., “Utilization of dual-source X-ray tomography for reduction of scanning time of wooden sample”, JINST Volume: 10 Article Number: C05008 (2015) (IF=1.366)

- J. Jakůbek, M. Jakůbek, M. Platkevič, P. Soukup, D. Tureček, V. Sýkora, D. Vavřík, "Large area pixel detector WIDEPIX with full area sensitivity composed of 100 Timepix assemblies with edgeless sensors", JINST 9 C04018 (2014) (IF=1.366)

- D. Vavřík, M. Holík, J. Jakůbek, M. Jakůbek, V. Kraus, F. Krejčí, P. Soukup, D. Tureček, J. Vacík, J. Žemlička, "Modular pixelated detector system with the spectroscopic capability and fast parallel read-out ", Journal of Instrumentation 9 C06006 (2014) (IF=1.366)

- Jandejsek, J. Jakůbek, M. Jakůbek, P. Průcha, F. Krejčí, P. Soukup, D. Tureček, D. Vavřík, J. Žemlička, "X-ray inspection of composite materials for aircraft structures using detectors of Medipix type", Journal of Instrumentation 9 C05062 (2014)

- E. Heijne, R. Ballabriga, M. Campbell, C. Leroy, X. Llopart, J. Martin, S. Pospíšil, J. Šolc, P. Soueid, M. Suk, L. Tlustos, D. Tureček, Z. Vykydal, W. Wong, "Measuring radiation environment in LHC or anywhere else, on your computer screen with Medipix", Nucl. Instr. and Meth. A, In press, doi:10.1016/j.nima.2012.05.023 (2013) (IF=1.433)

- Z. Vykydal, M. Holík, V. Kraus, S. Pospíšil, J. Šolc, D. Tureček, "A Highly Miniaturized and Sensitive Thermal Neutron Detector for Space Applications", Amer. Inst. of Physics (AIP) Conf. Proc., Volume: 1423, Pages: 393-396, doi: 10.1063/1.3688833 (2012) (IF=1.587)

- N. Stoffle, L. Pinsky, S. Hoang, J. Idarraga, M. Kroupa, J. Jakůbek, D. Tureček, S. Pospíšil, "Initial results on charge and velocity discrimination for heavy ions using silicon-Timepix detectors", Journal of Instrumentation (2012) (IF=1.366)

- D. Tureček, T. Holý, J. Jakůbek, S. Pospíšil, Z. Vykydal, "Pixelman: a multi-platform data acquisition and processing software package for Medipix2, Timepix and Medipix3 detectors ", Journal of Instrumentation 6 C01046, doi: 10.1088 / 1748-0221/6/01/C01046 (2011) (IF=1.366)

- D. Tureček, T. Holý, S. Pospíšil, Z. Vykydal, "Remote control of ATLAS-MPX Network and Data Visualization", Nucl. Instr. and Meth. A, Volume 633, Supplement 1, Pages: S45-S47, doi: 10.1016/j.nima.2010.06.117 (2011) (IF=1.433)

- D. Tureček, L. Pinsky, J. Jakůbek, Z. Vykydal, N. Stoffle, S. Pospíšil, "Small Dosimeter based on Timepix device for International Space Station", Journal of Instrumentation 6 C12037, doi: 10.1088/1748-0221/6/12/C12037 (2011) (IF=1.366)

- R. Ballabriga, G. Blaj, M. Campbell, M. Fiederle, D. Greiffenberg, E. Heijne, X. Llopart, R. Plackett, S. Procz, L. Tlustos, D. Tureček, W. Wong, "Characterization of the Medipix3 pixel readout chip", Journal of Instrumentation 6 C01052, doi: 10.1088 /1748-0221 /6/01 /C01052 (2011) (IF=1.366)

- J. Bouchami, F. Dallaire, A. Gutierrez, J. Idárraga, V. Král, C. Leroy, S. Pickard, S. Pospíšil, O. Scallon, J. Šolc, M. Suk, D. Tureček, Z. Vykydal, J. Žemlička, "Estimate of the neutron fields in ATLAS based on ATLAS-MPX detectors data", Journal of Instrumentation 6 C01042, doi: 10.1088/1748-0221/6/01/C01042 (2011) (IF=1.366)

- E. Gimenez, R. Ballabriga, M. Campbell, X. Llopart, I. Horswell, J. Marchal, K. Sawhney, N. Tartoni, D. Tureček, "Study of charge-sharing in MEDIPIX3 using a microfocused synchrotron beam", Journal of Instrumentation 6 C01031, doi: 10.1088/1748-0221/6/01/C01031 (2011) (IF=1.366)

- E. Heijne, R. Ballabriga, D. Boltje, M. Campbell, J. Idarraga, J. Jakůbek, C. Leroy, X. Llopart, L. Tlustos, R. Plackett, S. Pospíšil, D. Tureček, J. Vermeulen, J. Visschers, J. Visser, Z. Vykydal, W. Wong, "Vectors and submicron precision: redundancy and 3D stacking in silicon pixel detectors", Journal of Instrumentation 5 C06004, doi: 10.1088/1748-0221/5/06/C06004 (2010) (IF=1.366)

Publications without impact factor:

- Pinsky L., Hoang S., Idarraga-Munoz J., Turecek D., et al., "Summary of the First Year of Medipix-Based Space Radiation Monitors on the ISS", IEEE Aerospace Conference Location: Big Sky, MT Date: MAR 01-08, 2014
- C. Granja, M. Holík, J. Jakůbek, V. Kraus, T. Kuwahara, M. Platkevič, S. Pospíšil, D. Tureček, O. Valach, Z. Vykydal, "Timepix-based Miniaturized Radiation Micro-Tracker for the Micro-Satellite RISESAT", Transactions of JSASS, Aerospace Technology Japan, Vol. 12 No. doi: http://dx.doi.org/10.2322/tastj.12.Tr7 (2014)
- L. Pinsky, J. Jakůbek, Z. Vykydal, D. Tureček, S. Pospíšil, . et al. , "Preparing for the first Medipix detectors in space", 2012 IEEE Aerospace Conference Proceedings, doi: 10.1109/AERO.2012.6187011
- D. Tureček, J. Jakůbek, M. Kroupa, P. Soukup, "Energy calibration of pixel detector working in Time-Over-Threshold mode using test pulses", Nuclear Science Symposium and Medical Imaging Conference (NSS/MIC), IEEE (2011)
- E. Gimenez, R. Ballabriga, M. Campbell, I. Horswell, X. Llopart, J. Marchal, K. Sawhney, N. Tartoni, D. Tureček, "Characterization of Medipix3 With Synchrotron Radiation", Nuclear Science Symposium Conference Record (NSS/MIC), 2010 IEEE, On p 1976-1980 (2011)
- E. Gimenez, R. Ballabriga, M. Campbell, I. Dolbnya, I. Horswell, X. Llopart, J. Marchal, K. Sawhney, N. Tartoni, D. Tureček, "Evaluation of the radiation hardness and charge summing mode of a medipix3-based detector with synchrotron radiation", IEEE Nuclear Science Symposium Conference Record (2010)
- J. Bouchami, A. Gutierrez, C. Leroy, T. Holý, S. Pospíšil, M. Suk, J. Šolc, D. Tureček, Z. Vykydal, "Perspectives with the Medipix2-based Detectors Network in Atlas", 11th ICATPP 2009 Conference Proceedings, Pages: 155–162, doi: 10.1142/9789814307529_0027

List of Figures

List of Tables